ENVIRONMENTAL RESEARCH
LETTERS



**ACCEPTED MANUSCRIPT • OPEN ACCESS**

# A quantitative evaluation of forest aboveground biomass density map products in Oregon, USA

To cite this article before publication: Andrew Thomas Hudak *et al* 2026 *Environ. Res. Lett.* in press https://doi.org/10.1088/1748-9326/ae8b04

# A quantitative evaluation of forest aboveground biomass density map products in Oregon, USA

Andrew T. Hudak[1,*], Jennifer L. Bakken[2], Andrew Lister[3], Francisco Mauro[4], Matthew J. Gregory[5], Karin Riley[6], Barry Wilson[7], Maurizio Santoro[8], Sean Healey[2], Lei Ma[9], Yifan Yu[10], Benjamin C. Bright[1], John Byrne[1], Roy Mita[11], Rachel M. Houtman[6], John D. Shaw[2], Patrick A. Fekety[12], Grant Domke[7], Brian Walters[7], David M. Bell[13], Aaron Weiskittel[14], Jeff W. Atkins[15], Laura Duncanson[9], Neha Hunka[16], Robert Kennedy[5], Chad Babcock[17], Sassan Saatchi[10], Brett Raczka[18], Carlos Silva[19], Hao Tang[20] and George Hurtt[9]

1 USFS Rocky Mountain Research Station, Moscow, ID, USA
2 USFS Rocky Mountain Research Station, Ogden, UT, USA
3 USFS Northern Research Station, York, PA, USA
4 Universidad de Valladolid, Soria, Spain
5 Oregon State University, Corvallis, OR, USA
6 USFS Rocky Mountain Research Station, Missoula, MT, USA
7 USFS Northern Research Station, St. Paul, MN, USA
8 Gamma Remote Sensing, Muri bei Bern, Switzerland
9 University of Maryland, College Park, MD, USA
10 Jet Propulsion Laboratory, Pasadena, CA, USA
11 NFS National Applications Liaison Office, Fort Collins, CO, USA
12 Colorado State University, Fort Collins, CO, USA
13 USFS Pacific Northwest Research Station, Corvallis, OR, USA
14 University of Maine, Orono, ME, USA
15 Virginia Commonwealth University, Richmond, VA, USA
16 European Space Agency, Rome, Italy
17 University of Minnesota, St. Paul, MN, USA
18 National Center for Atmospheric Research, Boulder, CO, USA
19 University of Florida, Gainesville, FL, USA
20 National University of Singapore, Singapore, SG

*Corresponding Author; E-mail: andrew.hudak@usda.gov

Keywords: carbon monitoring system, Landsat, lidar, remote sensing, synthetic aperture radar

**Abstract**

Maps of Aboveground Biomass Density (AGBD) estimated from remote sensing data with models trained from inventory data are essential for carbon monitoring. Forest inventory plots in the United States (US) are measured by the Forest Inventory and Analysis (FIA) program of the US Forest Service (USFS). These plots are spatially representative, design unbiased, and provide estimates of AGBD and other forest attributes over large spatial domains, but do not provide spatially continuous or sufficiently precise estimates over small spatial domains (e.g., forest stands). Integration with remote sensing can fill this gap, but remote sensing cannot measure AGBD directly, so models of ground-measured AGBD as a function of remote sensing data are often used to generate synoptic maps. We evaluated 10 alternative types of AGBD maps that used lidar, multispectral satellite (Landsat) image time series, synthetic aperture radar (SAR), or alternative modeling approaches. We evaluated the agreement between mapped AGBD predictions and AGBD observations collected at the FIA plots or in stands surveyed on USFS lands. Ground observations were regressed on mapped AGBD predictions at different spatial aggregation levels: county, 64,000 ha FIA sample hexagon, stand polygon, FIA plot, and FIA subplot (unaggregated). The best linear regression model fit statistics were calculated and compared to evaluate the map products across the study area, a large portion of western and central Oregon. Based on these fit statistics, we found that the Landsat-derived maps performed best at the coarser evaluation levels (county, hexagon), airborne lidar-based products performed best at finer evaluation levels (stand, plot, subplot), and the SAR-dominated products showed lower agreement with ground-based AGBD estimates in this high-biomass Oregon study area. When choosing between AGBD map types, we recommend map users consider the scale of their decision space as much as type of remote sensing data or modeling approach used in production.

**Social media abstract**

All 10 alternative forest biomass maps compared in Oregon have utility but the best map to choose depends on user objectives and their scale of interest.

## 1. Introduction

Interest in forest carbon management has grown in recent decades due to concerns about impacts of human activities, climate change, and natural disasters on forest sustainability. In addition, private markets trading forest carbon offset credits as a form of nature-based climate solution have increased in scope in recent years. Aboveground tree biomass is a major part of the forest carbon pool, and monitoring, reporting, and verification (MRV) are necessary components of a carbon monitoring system (Hurtt et al 2022). Tree biomass is typically estimated using regression models as a function of species or species group, tree diameter and potentially height (Jenkins et al 2003). For forest inventory or remote sensing applications, the tree-level biomass estimates are most often summed for each plot and then divided by the plot area to calculate forest aboveground biomass density (AGBD, typically expressed in units of $Mg \cdot ha^{-1}$), and these plot-level data are used to make population-level estimates using sample-based estimation or as reference data for remote sensing applications.

Forest monitoring reporting frameworks, such as the United Nations Reducing Emissions from Deforestation and Forest Degradation program (REDD), consider sample-based estimation of AGBD or other attributes to be a best practice (IPCC 2019). At the country-level, this is often done through a national forest inventory (NFI), which is designed to provide probability-based estimates of relevant forest metrics. NFIs have provided the fundamental inputs for global forest assessments and monitoring efforts (Tomppo et al 2010). The 2020 United Nations Food and Agricultural Organization (FAO) Forest Resources Assessment (FRA) considered 236 countries, of which 150 had NFIs (Nesha et al 2021). These NFIs are considered complete in 120 countries, and only 41 countries have full NFIs that are updated at regular 5-10 year intervals (Nesha et al 2022).

AGBD maps are used across a range of scales, such as by forest managers operating at project scales where NFI plots are too sparse to represent local conditions, ecosystem modelers working at landscape-regional scales (Raczka et al 2021, Huo et al 2024), and by policy makers at national scales (Tinkham et al 2018). One challenge associated with AGBD reporting is uncertainty quantification, however many AGBD maps may only report modeling error. Other sources of uncertainty in ground data include measurement error, sampling error, allometric error, and spatial referencing error (Fortin 2021; Kennedy et al 2024; Yanai et al 2020; Yanai et al 2023); those in remote sensing data include atmospheric effects, sensor gains/offsets, and georeferencing errors (Curran and Hay 1986; Yanai et al 2020; Fortin 2021). When using ground data and remote sensing for estimation, these errors can be propagated when upscaling pixel-level estimates. Errors that reduce map precision (e.g., georeferencing error) will average out upon aggregation, but errors that may introduce bias in estimators (e.g., allometric error) will not. Precision and accuracy assessment of spatial products are therefore critical components of monitoring strategies that rely on maps produced through predictive modelling with remote sensing and ground data.

Several alternative AGBD map products have been developed to support carbon accounting efforts in the United States (US), with much thanks to directed funding from the NASA Carbon Monitoring Systems (CMS) Program (Hurtt et al 2022) and investment by the US Forest Service (USFS), the federal land management agency charged with managing USFS National Forest System (NFS) lands, and with collecting and maintaining the NFI data for the US through the Forest Inventory and Analysis (FIA) Program. AGBD maps support carbon accounting since aboveground carbon density (AGCD) is typically estimated as 50% of AGBD, although this is now considered an oversimplification (Doraisami et al 2024). AGBD map products also provide synthetic estimates that are used to help quantify forest carbon status and flux (Bullock et al 2023; Hurtt et al 2024). Emerging carbon markets contribute to the proliferation of AGBD (or AGCD) maps, such that forest managers are faced with a choice. Which of several alternative AGBD maps might best meet a forest manager's objectives, and why? Our primary objective is to evaluate AGBD map types by comparing the mapped AGBD to ground observations of AGBD, which are sometimes considered as ground “truth” because they are based on physical tree measurements, but in reality these estimates are also subject to measurement, sampling, and allometric errors (Johnson et al 2025). A secondary objective is to demonstrate a framework for evaluating current (and future) AGBD maps and associated uncertainties. Since all of the AGBD estimates considered have already been published, the novelty of the study lies in the assessment scales afforded by the ground observations, varying from small administrative units (counties) down to field plot (and subplot) levels, effectively bracketing the scales where most forest management decisions are made.

Counties are a convenient, well-understood, often management-relevant reporting unit in many regions. However, county boundaries are irregular in size and shape, making their utility as consistent, comparable aggregation units difficult. Our second analysis unit is a set of 64,000-ha hexagons derived from a tessellation created for the Environmental Protection Agency’s Environmental Monitoring and Assessment Program (EMAP) (White et al 1992). EMAP hexagons are smaller than most counties and are consistent in size and shape, with sufficient area to generally have enough plots containing forest (e.g., approximately 30/hexagon in Oregon) to represent the status of AGBD at the 64,000 ha scale (Menlove and Healey 2020).

The smallest polygon units considered in our study represent individual forest stands, which were extracted from a polygonal segmentation of forest stands on USFS NFS lands. The segmentation of the forest into stands is meant to support ecological classification and forest management goals, with stands representing homogeneous areas. Stand-level data include, among other things, summaries of tree lists generally collected in variable-radius subplots systematically laid out along transects meant to represent the stand. Because the stand data are not a census of all trees within them, sampling error exists in these estimates as well.

There are four major assumptions underlying our evaluation: 1) Because ground estimates of AGBD at the county and hexagon scales are summarized from design-based FIA plots, we considered them unbiased at the spatial extent of counties and hexagons. Similarly, because the stand-level estimates are derived from stand examination subplots measured for the same stand units, we considered them unbiased with regard to the stand polygons they represent. 2) Our analysis methods are not adversely affected by variation in size and shape of county and stand polygons; i.e., each analysis unit has equal weight, regardless of size and shape. 3) Validating maps at a 30-m pixel resolution using a larger aggregation unit, namely counties and hexagons, can inform users as to the appropriate use of the maps at that scale. Such an analysis may not provide the information required for projects with significantly smaller or larger analysis units. In other words, a hexagon-level validation statistic might not be relevant if the map is meant to be used to guide decisions for sub-hexagon scale geographies. 4) The fit statistics used to evaluate the models used to generate AGBD estimates assume independent AGBD ground observations. Across all AGBD maps considered, this assumption only held for the stand level evaluation and was usually violated in the case of the other evaluation levels, as we will discuss.

## 2. Materials and Methods

### 2.1 Study Area

The study area includes the area within the state of Oregon (OR) matching the spatial extent of 20 lidar coverages (figure 1A). OR is 66,695 km$^2$ in area and has extensive lidar coverage, which spans large topographic and climatic gradients that typify the western USA and influence diversity and productivity (Peterson and Waring 1994). As a result, OR includes forests that cover the majority of the range in AGBD in western North America (Hicke et al 2007). In Figure 1B, the FIA plots can be seen in relation to the study area (grey) and hexagon boundaries.

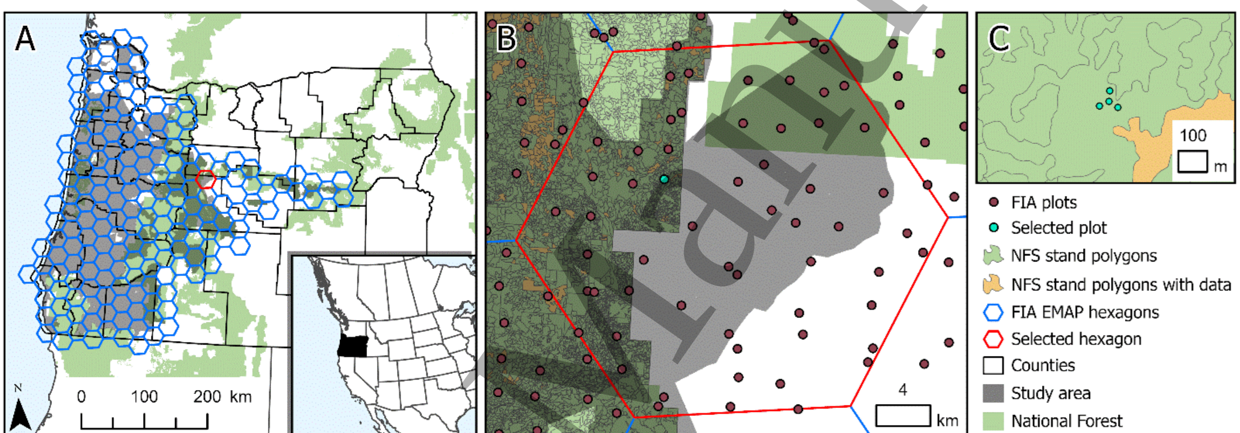


**Figure 1.** A) Study area in Oregon, USA, consisting of a patchwork of 20 airborne lidar collections, which matches the study area of Mauro et al (2021b), the smallest common area across the 10 Aboveground Biomass Density (AGBD) map products compared. B) The FIA EMAP hexagon selected for illustration purposes; the publicly available FIA plot locations shown are perturbed; i.e., not the accurate but confidential plot locations used in the analysis. C) The FIA plot selected for illustration purposes; each FIA plot has this same configuration of 4 subplots. FIA plots have no relationship to NFS stands. EMAP: Environmental Monitoring and Assessment Program; FIA: Forest Inventory and Analysis; NFS: National Forest System.

In FIA estimation, these hexagons (and often counties) are treated as classification variables, often called "domains". Domains are variables that provide labels to plots, portions of plots, or trees, and are used in the estimation process to partition the estimate, in our case, into hexagon- or county-level estimates. Estimates of total AGB are created for a given hexagon by first assigning a zero value to plots in the stratum that are not in the hexagon being evaluated, then calculating the mean AGBD of all plots (zero and nonzero) in the stratum, and then multiplying by the known area of the stratum. This forms the numerator of the AGBD ratio estimate. Next, a similar calculation method is performed with the values of proportion forest per plot to calculate the estimate of total forest area (the denominator of the ratio estimate) for that hexagon. The AGBD estimate for the hexagon is formed by dividing the total AGB estimate by the estimate of total forest area to arrive at biomass/hectare of forest land. These calculations are adjusted in various ways to account for estimation units with multiple strata and partial nonresponse as described in Bechtold and Patterson (2005). It is important to note that this approach is not equivalent to simply calculating the average of the plot-level AGBD values for each hexagon. The implications of adopting the FIA approach (which is designed for population-level estimation and accommodates domain estimation) are that variations in nonresponse proportion by stratum, stratum weights, and stochasticity of sampling intensity due to the FIA sample selection procedure add uncertainty to hexagon- and county-level estimates, relative to what would be achieved if there were a more deterministic sample design aimed at making hexagon- or county-level estimates. Nonetheless, the FIA sampling strategy is unbiased when adopting the domain paradigm described above.

It can be noted in figure 1B that not all FIA plots are in the grey study area; some are in forest (green) but outside of the study area, and these plots contributed to the average for that hexagon. However, the map-based biomass/hectare is based on pixels averaged across both the grey and the grey/green (overlap) areas. Therefore, for that hexagon that only partially intersects the study area, we were forced to assume that the biomass density in the green area is not substantially different from that in the grey or grey/green areas combined, when comparing means at the hexagon level. A similar assumption was required for the county-based level comparisons. Where this assumption does not match reality, the relationship between predicted and observed AGBD estimates at the county and hexagon aggregation levels will be weakened. While this situation is not ideal, we proceeded in this manner because one of our goals is to elucidate practical difficulties that users might encounter when using the publicly available FIA data to validate maps. Because the public FIA plot coordinates are spatially perturbed, there is no way the public can assess whether a particular plot is precisely in the study area or not.

**2.2 General approach and assumptions**

The methodological approach of our study is to compare ground-based AGBD observations to aggregations of AGBD estimates from ten candidate AGBD map products across much of the forested (mostly western) portion of OR at 6 geographic scales. GIS layers representing these scales include, first, 3 polygon levels ranging from counties (639,000 ha on average in our study area) to hexagons (64,000 ha) to delineated stands (18.3 ha on average in our study area) on USFS NFS lands, and second, 3 point levels representing FIA plots (each comprised of 4 subplots), unaggregated subplots, and the central subplot of each FIA plot.

**2.3 Aboveground Biomass Density (AGBD) Maps**

We considered 10 AGBD map products that differed in at least 3 fundamental respects: remote sensing data source(s), reference data for model training, or modeling approach. The AGBD map produced by Mauro et al (2021b) represents the smallest spatial extent of the 10 AGBD maps considered, so we used it as a mask to define the study area. Therefore, we clipped the other 9 AGBD map products to the same mask to ensure equitable comparisons across the study area (figure 1). Various features of the different map pedigrees were difficult to standardize among all 10 maps but could be more readily interpreted through 5 pairs of similar AGBD map comparisons, which also made for a more digestible and compelling narrative. The essential characteristics of the 10 AGBD map products are summarized in table 1, followed by the distinguishing characteristics of the 5 pairs of similar AGBD maps compared.

**Table 1.** Key characteristics of the 10 Aboveground Biomass Density (AGBD) maps evaluated.

| | AGBD Map | Training Data | Live and Dead Diameter at Breast Height (DBH) Thresholds of Trees Used for Model Training | Spatial Resolu-tion | Temporal Resolu-tion | Original Units | Pixel-Level Model Un-certainty Metric | Fo |
|---|---|---|---|---|---|---|---|---|
| [1] | OR-LIDAR | FIA plots | Live >= 2.5 cm dbh, Dead >= 12.7 cm dbh | 30 m | lidar collection date | Mg ha$^{-1}$ | Standard de-viation | No |
| [2] | CMS-LIDAR | Stakeholder-contributed plots | Live and Dead >= 12.7 cm dbh | 30 m | lidar collection date | Mg ha$^{-1}$ | Standard de-viation | No |
| [3] | CMS-AGB | Random sample of uncalibrated CMS-LIDAR map estimates | Trained from CMS-LIDAR estimates, which used Live and Dead >= 12.7 cm dbh | 30 m | annual (2000-2016) | Mg ha$^{-1}$ | Standard de-viation | PA |
| [4] | GNN | FIA plots | By default, Live >= 2.5 cm dbh, Dead >= 12.7 cm dbh; for this study, the same Live and Dead >= 12.7 cm dbh as used for the CMS-AGB maps | 30 m | annual (1990-2017) | kg ha$^{-1}$ | Standard de-viation | By sys F/N |
| [5] | TreeMap | FIA plots | Live >= 2.5 cm dbh, Dead >= 12.7 cm dbh | 30 m | 2016 | tons C acre$^{-1}$ | N/A | LA co |
| [6] | BIGMAP | FIA plots | Live >= 2.5 cm dbh, Dead >= 12.7 cm dbh | 30 m | Circa 2016 (2014-2018) | tons C pixel$^{-1}$ | N/A | Co ba po |
| [7] | MAXENT | FIA plots | Live >= 2.5 cm dbh, Dead >= 12.7 cm dbh | 100 m | 2005, 2010, 2015, 2016, 2017 | Mg C ha$^{-1}$ | Standard de-viation | 20 |
| [8] | ESACCI | Not plots, but subnational forest AGBD statistics | N/A | 100 m | 2010, 2017, 2018, 2019, 2020 | Mg ha$^{-1}$ | Standard de-viation | No |
| [9] | ED | Not plots, but global EDv3 model and satellite lidar observations | N/A | ~1,113 m | Circa 2020 (2018-10-01 to 2021-10-01) | kg C m$^{-2}$ | N/A | No |
| [10] | GEDI | Stakeholder-contributed plots at footprint level, then rasterized us-ing hybrid model-based inference | N/A | 1000 m | Circa 2020 (2019-04-18 to 2021-08-04) | Mg ha$^{-1}$ | Standard er-ror, based on number of footprints | No |

[1] https://wifire-data.sdsc.edu/dataset/above-ground-biomass-agb
[2] https://daac.ornl.gov/cgi-bin/dsviewer.pl?ds_id=1766
[3] https://daac.ornl.gov/cgi-bin/dsviewer.pl?ds_id=1719

[4] https://lemma.forestry.oregonstate.edu/data/structure-maps
[5] https://www.fs.usda.gov/rds/archive/Catalog/RDS-2021-0074
[6] https://fia-usfs.hub.arcgis.com/
[7] https://daac.ornl.gov/cgi-bin/dsviewer.pl?ds_id=1752
[8] https://catalogue.ceda.ac.uk/uuid/af60720c1e404a9e9d2c145d2b2ead4e/
[9] https://daac.ornl.gov/CMS/guides/CMS_Global_Forest_AGC.html#qualityassess
[10] https://daac.ornl.gov/GEDI/guides/GEDI_L4B_Gridded_Biomass.html

2.3.1. OR-LIDAR and CMS-LIDAR

The OR-LIDAR and CMS-LIDAR AGBD map products most heavily leverage airborne lidar, long and widely regarded as the best available remote sensing data source for characterizing forest structure attributes (Lefsky et al 2001, Hudak et al 2009), including AGBD. Both map products were composed of AGBD estimates at 30 m resolution made using Random Forest (RF) regression models. Mauro et al (2021b) predicted AGBD across the extent of 20 lidar collections in OR (OR-LIDAR; dataset: Mauro et al 2021a), within which 1133 design-based FIA plots were available to train the model. Hudak et al (2020) predicted AGBD across a larger spatial extent of 176 lidar project areas and 3805 forest inventory plots collected and contributed by stakeholders spread across OR and neighboring Washington (WA) and Idaho (ID) (dataset: Fekety et al 2025). Because the CMS-LIDAR AGBD map was trained from stakeholder-contributed plot data that are neither standardized nor spatially balanced, it is subject to biases, thus the CMS-LIDAR AGBD map was calibrated using spatially balanced FIA subplot-level AGBD estimates within the lidar project areas in OR, WA, ID and western Montana (MT). Simple linear models regressing FIA subplot estimates on the uncalibrated CMS-LIDAR estimates were fit for each state and applied. The stakeholder-contributed plot data used to train CMS-LIDAR often omitted saplings, such that only live and dead trees with diameter at breast height (dbh) $\geq$12.70 cm were available for model training, and this constraint propagated to the CMS-AGB product (see below) trained from CMS-LIDAR (table 1).

2.3.2. CMS-AGB and GNN

CMS-AGB and GNN are the only products that consist of annual AGBD maps. They leverage Landsat imagery and derived layers fitted on an annual time step from Landsat time series processed with the LandTrendr algorithm (Kennedy et al 2010). Besides LandTrendr metrics, topographic metrics and climate metrics derived from 30-year climate normals were also used as predictors. The main difference is that CMS-AGB was trained from a stratified random sample of the uncalibrated CMS-LIDAR AGBD estimates (see above), whereas GNN was trained directly from FIA plot data.

Because CMS-AGB was not trained from design-based FIA data, the annual AGBD maps were calibrated using same-year, annual estimates of AGBD covering the CMS-AGB study area (OR, WA, ID and western MT), obtained from FIA data using EVALIDator (https://apps.fs.usda.gov/fiadb-api/evalidator). EVALIDator is a web-based tool that allows users to produce population estimates for common forest attributes. These estimates were regressed on the uncalibrated AGBD map estimates assumed to be biased. A single simple linear regression model was fit and applied to calibrate the annual AGBD maps to match FIA estimates for the entire northwestern USA region. (Hudak et al 2020, dataset: Fekety et al 2019).

Unlike CMS-AGB, the GNN model did not use RF but rather GNN imputation (Ohmann and

Gregory 2002, Ohmann et al 2012), which is based on a canonical correspondence analysis ordination that associates the AGBD response with the LandTrendr, climatic, and topographic predictors along ecological gradients (Kennedy et al 2018, dataset: https://lemmadownload.forestry.oregonstate.edu). To facilitate comparison to CMS-AGB maps for this analysis, FIA tree lists used for GNN predictions were subset to the same minimum dbh threshold of 12.70 cm for both live and dead trees (table 1). By default, the forest/nonforest (F/NF) mask is based on the GAP/LANDFIRE national ecosystems map (Davidson and McKerrow 2016), but for this analysis the same 2009 PALSAR F/NF mask was used as for the CMS-AGB maps, to control for another variable that could confound the comparison.

2.3.3. TreeMap and BIGMAP

These two conterminous US (CONUS) AGBD map products both involve the imputation of one or more nearest neighbor FIA plots to each pixel to form the basis of a synthetic estimator. TreeMap, which is based on one nearest neighbor plot ($k$=1), was produced by the Missoula Fire Sciences Lab, while BIGMAP is based on multiple nearest neighbor plots ($k$>1) and was produced by the FIA program. BIGMAP used field plots and imagery collected from 2014-2018, while TreeMap used 2016 imagery and plot observations collected from 2004-2017. Neither report pixel-level model uncertainty because neither modeling approach supply this by default. In addition, the developers of both maps assert that model error comprises only one of several sources of error in the estimates, and as such likely underrepresents the true error they might attempt to report.

TreeMap uses RF for imputation of FIA plot data based on a suite of location, topographic, vegetation (Existing Vegetation Cover, Existing Vegetation Height, and Existing Vegetation Type from LANDFIRE), biophysical, and disturbance variables (Riley et al 2021a). Based on this suite of predictor variables, the RF model assigns the FIA plot estimate that is most similar to each pixel (Riley et al 2021b, Riley et al 2022). Therefore, the TreeMap dataset consists of a 30m CONUS map of FIA plot IDs, which can be linked to attributes in the FIA databases (including lists of trees), allowing estimation of many attributes, including AGBD (dataset: Riley et al 2021a). The F/NF mask is based on LANDFIRE Existing Vegetation Cover (Rollins 2009, La Puma 2023), where pixels having >=10% tree cover were defined as forest (table 1). We calculated AGBD from TreeMap 2016 by summing the CARBON_L (live aboveground carbon in trees greater than 2.54 cm dbh) and CARBON_D (dead aboveground carbon in trees greater than 12.70 cm dbh) fields in the attribute table of the raster and multiplying the total by two. The CARBON_L and CARBON_D estimates are produced by summing FIA estimates for the bole, top, and stump for individual trees and saplings and converting to tons-per-acre figures (Riley et al 2022). TreeMap estimates are in units of biomass carbon density (i.e., tons/acre) that we multiplied by 2.2417 to convert to Mg/ha and again by 2 to calculate AGBD.

BIGMAP (Big Data, Mapping, and Analytics Platform) is a cloud-based modeling environment developed by FIA to produce up-to-date maps of AGBD and other forest attributes. The precursor to the BIGMAP products were 250m pixel resolution maps based on Moderate Resolution Imaging Spectroradiometer (MODIS) imagery, but BIGMAP products used in this study are based on derivatives of 30m resolution Landsat image time series. Image-derived tasseled cap (TC) indices were produced for each pixel for each image collected during the 2014-2018 epoch with the assumption that the TC time series represents the seasonal cycles in vegetation phenology. The series of TC images was modeled using harmonic regression, and the coefficients from this regression were then, along with topographic and climate maps, used to create the equations for canonical variates with canonical correspondence analysis. These equations were applied to the TC, climate and topographic map data as a data reduction and feature extraction technique to generate predictor layers used in the *k* Nearest Neighbor (*k*NN) imputation (Ohmann and Gregory 2002, Wilson et al 2012, 2013, 2018).

BIGMAP is provided as an image service (dataset: https://fia-usfs.hub.arcgis.com/), where biomass carbon is not provided in units of carbon density but rather in carbon mass per pixel. Maps are provided in Web Mercator projection with the intention of facilitating their provision to users. However, this projection leads to variation of pixel area with latitude across CONUS. In OR, the Web Mercator pixel area scale factor ranges from ~1.8 in the south to ~2.0 in the north, meaning that the pixel area is nearly twice as large as the nominal pixel area of 900m$^2$. Therefore, the BIGMAP pixel aboveground carbon (AGC) mass value is divided by 0.09 (the nominal pixel area in hectares) and then again by 1.9 (the mean pixel area scale factor) to calculate AGCD, and finally is multiplied by 2 to convert AGCD to AGBD. Separate BIGMAP rasters for live tree and dead tree carbon were downloaded and summed and used to create AGBD as described above. The BIGMAP F/NF mask was formed by combining a F/NF reclassification of the 2016 US National Land Cover Datasets (NLCD) Land Cover/Land Use product with the BIGMAP predicted forest proportion (table 1). NLCD classes of open water, perennial ice/snow, developed, barren, herbaceous, and planted/cultivated pixels were masked out as nonforest; for remaining classes, the pixel was also masked out as nonforest if the predicted forest proportion was <0.5.

### 2.3.4. MAXENT and ESACCI

The MAXENT and ESACCI map products, with a spatial resolution of 100 m, are the only two AGBD maps that use (primarily) synthetic aperture radar (SAR). Both mapped AGBD in 5 different years, although only in 2010 are the map years the same (table 1).

The MAXENT map product (dataset: Yu et al 2021, Yu et al 2022) is so named by us because it uses a modified Maximum Entropy estimator (Phillips et al 2006, Phillips and Dudík 2008) to provide annual estimates of both live and dead AGBD across the CONUS for the years 2005, 2010, 2015, 2016, and 2017 (table 1). FIA plot data were used to train the model based on pixel-level site conditions characterized by remote sensing data inputs: Landsat multi-spectral, MODIS on board the AQUA satellite, microwave radar measurements from Phased Array type L-band Synthetic Aperture Radar (PALSAR) on Advanced Land Observation Satellite (ALOS) and

PALSAR-2 on ALOS-2, airborne imagery from National Agriculture Imagery Program (NAIP), and the digital elevation model from the Shuttle Radar Topography Mission (SRTM). These satellite and airborne remote sensing datasets were co-registered on a common 100 m (1 ha) grid.

The European Space Agency's (ESA) Climate Change Initiative (CCI) program has a Biomass CCI team that produced annual, global AGBD maps, named here simply ESACCI. Santoro et al (2021, 2024) derive AGBD from SAR data collected by, depending on the year, the Copernicus Sentinel-1 mission, Envisat's ASAR instrument, or JAXA's (ALOS-1 and ALOS-2). The pool of remote sensing data used to predict AGBD includes multi-temporal C- and L-band observations for all biomes and for all years. The inversion is based on a physical model that relates the SAR backscattered intensity to canopy height and canopy density. The relationship to AGB in the model is introduced by means of two forest structural functions that express canopy density as a function of canopy height and the latter as a function of AGBD. These functions are supported by global spaceborne LiDAR canopy density and height observations from the ICESat and ICESat-2 missions, and subnational forest inventory statistics of AGBD. Version 4 (considered here) consists of AGBD maps for the years 2010, 2017, 2018, 2019 and 2020 (table 1). Each ESACCI product consists of two global layers that include estimates of AGBD and AGBD uncertainty expressed as the standard deviation (dataset: Santoro and Cartus 2023).

#### 2.3.5. ED and GEDI

The Ecosystem Demography (ED) and GEDI map products both use spaceborne GEDI datasets, although ED considers GEDI and/or ICESat-2 observations, while the GEDI product considers GEDI observations alone. Both ED and GEDI are also well matched temporally, being single-time (circa 2020) data products conditioned on a three-year window of satellite lidar data availability (table 1).

The ED map product uses the global EDv3 ecosystem demography model (Ma et al 2022) and the Copernicus Global Land Service land cover product (Buchhorn et al 2020) to provide global estimates of forest aboveground carbon stocks at a 0.01-degree (~1.11 km) resolution (Ma et al 2023). The ED model simulations were driven by inputs that characterized meteorology, carbon dioxide levels, and soil properties, once initialized with lidar observations of tree canopy height collected by either GEDI or ICESat-2, the two NASA spaceborne lidar missions, or both sensors (table 1). Gridded canopy height histograms were generated from 3.77 billion lidar samples, then linked to ED simulations of canopy height and carbon dynamics during ecosystem succession. Although not publicly available with the data product (dataset: Ma et al 2022), pixel-level upper and lower bounds were estimated to represent the possible range of AGBD values between the onset of canopy height saturation and the modeled maximum AGBD, for pixels where lidar height exceeded the model-simulated maximum canopy height.

The GEDI L4B gridded map product provides AGBD estimates at 1 km resolution between 51.6°N and 51.6°S latitude (as restricted by the orbital reach of the International Space Station (ISS) on which GEDI is mounted), based on GEDI observations from 2019-04-18 to 2021-08-04.

The L4B product statistically infers mean AGBD from GEDI footprint-level AGBD samples (L4A footprint-level AGBD product) located within each 1 km cell, along with the standard error of the mean as the measure of uncertainty. This uncertainty includes both the error associated with modeling the L4A estimates of AGBD, and the sampling error because the L4A estimates are merely a sample of the 1 km grid cell (table 1). The AGBD estimates at footprint level used for training were fitted from stakeholder-contributed field plots within which airborne (discrete-return) lidar points were used to simulate the GEDI waveform (Kellner et al 2023). Patterson et al (2019) describes the hybrid model-based mode of inference used in the L4B product. More details regarding the gridding procedure are provided in the GEDI L4B Algorithm Theoretical Basis Document (Healey et al 2023).

Some scattered data gaps existed in the GEDI map, not by design, but because of the banding pattern in the distribution of GEDI footprints across the Earth's surface caused by a lower ISS orbit than was planned for the GEDI science mission. This translated into some pixels in the GEDI 1 km AGBD product having insufficient footprints between ISS orbital paths to inform an AGBD estimate (dataset: Dubayah et al 2022). We ignored these small, scattered NoData pixels in our evaluation, since we were aggregating AGBD pixels within larger polygons (except for some smaller stand polygons).

**2.4. Training Data**

The OR-LIDAR, CMS-LIDAR, CMS-AGB, and GNN maps were trained from plot-level AGBD estimates calculated from tree measurements summarized using the Fire and Fuels Extension of the Forest Vegetation Simulator (FFE-FVS) (Rebain 2025, Dixon 2025). The default FVS equations specified for the variants available in the northwestern USA produced AGBD estimates that can be 0-9% higher (depending on species and site) than the AGBD estimates used to train the TreeMap, BIGMAP, and MAXENT maps and calculated by FIA using the Component Ratio Method (CRM) (Woodall et al 2011), which converts cubic volume estimates to biomass using constant specific gravity values. The OR-LIDAR, TreeMap, BIGMAP, and MAXENT map products were trained using FIA reference data (table 1).

Stakeholder-contributed forest inventory plots were used to train the CMS-LIDAR product directly and the CMS-AGB product indirectly. Similarly, the gridded GEDI product (L2B) evaluated here is indirectly trained from globally contributed stakeholder plots via the L2A footprint-level GEDI product (not evaluated here) (table 1). The ESACCI and ED maps employed methodologies that did not require FIA or other inventory plot data for model training (table 1).

**2.5. Evaluation Data**

Plot-level FIA estimates based on CRM allometries were obtained from summaries of tree-level data available from the public FIA DataMart (https://research.fs.usda.gov/products/dataandtools/fia-datamart). Plot-level estimates were aggregated within county polygons and EMAP hexagons using the FIA EVALIDator tool, in a manner similar to the approach of Menlove and Healey (2020, 2021). FIA plots were assigned to hexagons based on the publicly available locations (longitude and latitude) that were perturbed to maintain confidentiality. Thus, plot locations can be perturbed out of a hexagon, adding a source of uncertainty to hexagon-level estimates, but not out of a county. FIA data summaries using data from the cycle spanning 2010-2019 were used to evaluate all AGBD maps at the county and hexagon levels. Standard errors in the AGBD observations were calculated based on the plot count per polygon.

Stand-level AGBD estimates come from stand inventory information maintained in the USFS Field Sampled Vegetation (FSVeg) database (https://www.fs.usda.gov/nrm/fsveg/index.shtml), which the USFS also maintains but separately from the FIA DataMart. Stand exam data from FSVeg were obtained from the USFS National Applications Liaison Office and linked by stand ID to NFS stand polygons from stand maps obtained for the 10 USFS National Forests that intersect our study area in OR. We did not use stands with estimates imputed by the FSVeg Spatial Data Analyzer, but rather only used stands where ground measurements were collected. Stand exam data were imported into the FFE-FVS to calculate carbon density (Mg C/ha), which was multiplied by 2 to calculate AGBD (Mg/ha). FSVeg stand data collected from 2000 to 2021 were used to evaluate all AGBD maps at the stand level. Standard errors in the stand-level AGBD observations are calculated based on the subplot count per stand.

The FIA and FSVeg tree data summarized to evaluate the CMS-LIDAR, CMS-AGB, and GNN products were constrained to include only live and dead trees with dbh $\geq$12.70 cm, matching the same condition imposed on the training data for these 3 map products. FFE-FVS was run twice, once including live saplings (minimum dbh $\geq$2.54 cm) to evaluate 7 of the 10 AGBD maps, and once excluding live saplings (minimum dbh $\geq$12.70 cm) to evaluate the other 3 AGBD maps (CMS-LIDAR, CMS-AGB, and GNN). In both runs, the geographically appropriate FVS variant was used based on the stand location.

FIA plot data collected from 2005 to 2019 were used to evaluate all AGBD maps at the plot and subplot levels based on accurate (but confidential) geolocations. The data were temporally filtered such that only plots that were measured within +/-3 years of the nominal date of the input imagery for a given map were considered.

### 2.6. AGBD Map Summarization

The 'zonalstats' function in ArcGIS was used to calculate the pixel count and mapped AGBD mean and standard deviation statistics per evaluation polygon (county, hexagon and stand). We did not calculate standard error based on pixel count per polygon because pixel counts per polygon can be orders of magnitude higher than FIA plot counts per polygon, which would provide an overly optimistic measure of confidence in the remote sensing estimate, primarily because it would wrongly assume lack of spatial autocorrelation between neighboring pixels (Kennedy et al 2024).

For the comparison of mapped AGBD estimates with FIA estimates at all 3 point levels, we considered subplots with any amount of forest. Subplot-level AGBD was estimated by aggregating tree data within each subplot containing forested conditions. Because we had access through a legal agreement to the confidential FIA plot center locations (which correspond to the centers of the central subplots), we could also calculate the center locations of the 3 peripheral subplots based on their separation distance (36.6 m) and azimuth (0, 120, or 240 degrees) from the center of the central subplot, while also accounting for magnetic declination (figure 1c). AGBD map pixel values were extracted at each subplot center location. For the plot-level analysis, we averaged, per plot, both the AGBD ground observations (among those subplots having forest) and extracted AGBD map pixel values. For the center-subplot-level analysis, we ignored the ground and mapped AGBD data from the 3 peripheral subplots.

**2.7. Evaluation Statistics**

Predictions from the AGBD maps were evaluated at the 3 polygon and 3 point levels. At the 3 polygon levels—county, hexagon, and stand—the aggregated AGBD pixel means were compared to ground-based estimates representing the same polygons, using simple scatterplots. Ground-based AGBD estimates were regressed on mapped AGBD estimates to evaluate map precision and accuracy. Traditional ordinary least squares (OLS) regression minimizes Root Mean Square Error (RMSE) but assumes no measurement errors in either the ground-based or remotely-sensed estimates (Cohen et al 2003). Therefore, standardized major axis (SMA) regression with the smatr package in R was used; SMA regression increases RMSE compared to OLS regression but more importantly acknowledges that both estimates of AGBD have measurement error (Warton et al 2006, 2012). We used Pearson correlation (r) to quantify correlation strength between ground-based AGBD and mapped AGBD estimates. RMSE combines the variance and squared bias of the set of residuals, making it a measure of precision and accuracy, respectively. We calculated mean Bias Error (MBE), the average difference between mapped and ground AGBD estimates, as the measure of bias that also indicates accuracy.

**3. Results**

USFS National Forests comprise a large proportion of federal lands, especially in western US states like OR, where NFS lands cover ~6.5M ha. Although only 29% of our study area was on NFS lands, there were still many more stand polygons (n = 3,496) than there were hexagons (n = 179) or counties (n = 24) intersecting our study area (table 2). For brevity, only stand-level scatterplots are illustrated here, due to the stand data being the only evaluation data completely independent from any training data (table 1), whereas all polygon-level fit statistics are summarized in table 2. Table 2 also includes fit statistics of observations regressed on predictions at the aggregation levels described above. Some AGBD map types had more than a single map available, in which case the mean AGBD prediction across all maps was calculated, with results summarized in table 2. A full accounting of the SMA regression fit statistics from every single AGBD map considered is available in table S1.

### 3.1. OR-LiDAR and CMS-LiDAR

Both OR-LIDAR and CMS-LIDAR overpredicted (positive MBE) AGBD across evaluation levels, except CMS-LIDAR underpredicted (negative MBE) AGBD at the coarser county and hexagon levels. OR-LIDAR had notably higher Pearson r, lower RMSE, and lower MBE at the county level (table 2A). At the stand level, the fit statistics were very similar (figure 2). At the 3 point evaluation levels (plot, all subplot, and center subplot), all fit statistics indicated consistently better performance by the OR-LIDAR map than the CMS-LIDAR map (table 2B).

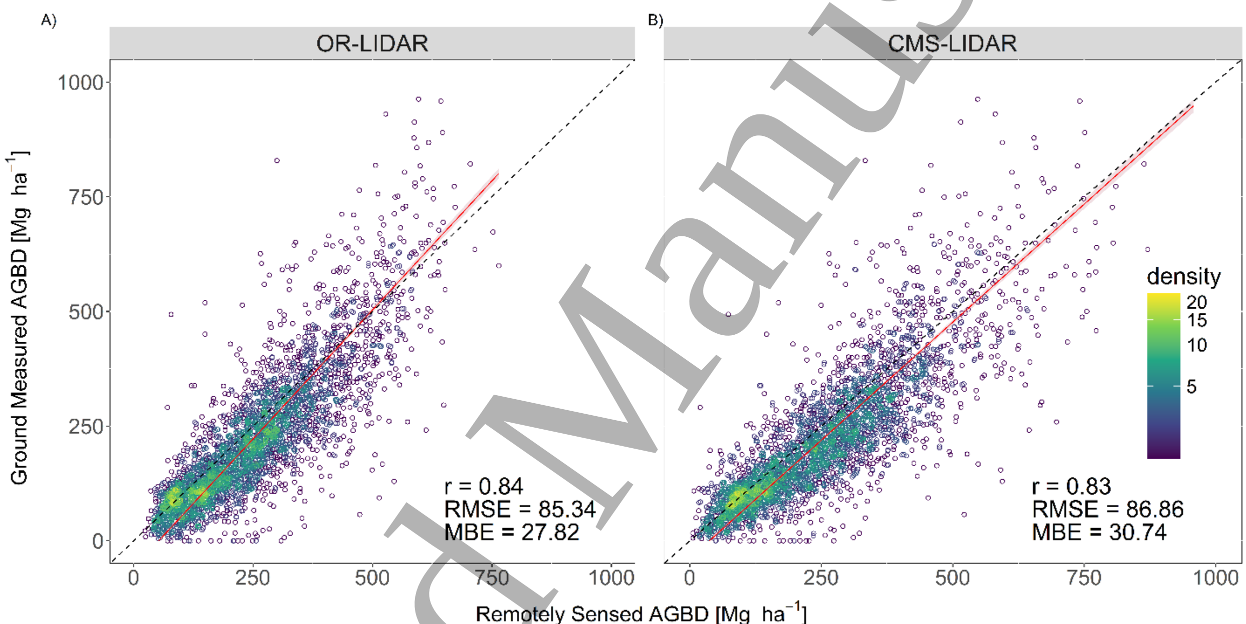


**Figure 2.** Ground-based AGBD observations regressed on mean AGBD estimates from A) OR-LIDAR and B) CMS-LIDAR maps after aggregation at the stand level. The pink shaded area around the red solid line of best fit represents the 95% confidence interval. AGBD: Aboveground Biomass Density.

### 3.2. CMS-AGB and GNN

Both the regional CMS-AGB and GNN maps always underpredicted (negative MBE) AGBD across all evaluation levels. GNN achieved higher r and lower RMSE than CMS-AGB, suggesting better overall accuracy, while CMS-AGB had lower MBE, suggesting less bias (figure 3, table 2). These differences in MBE were more pronounced at the 3 polygon evaluation levels whereas differences in Pearson r and RMSE were more obvious at the 3 point evaluation levels (table 2). Within both the CMS-AGB and GNN time series, the 17 annual AGBD maps trended towards less bias (lower MBE), as mapped AGBD estimates slowly increased from 2000-2016, while the ground-based estimates did not. Meanwhile, the r and RMSE statistics remained very stable (table S1).

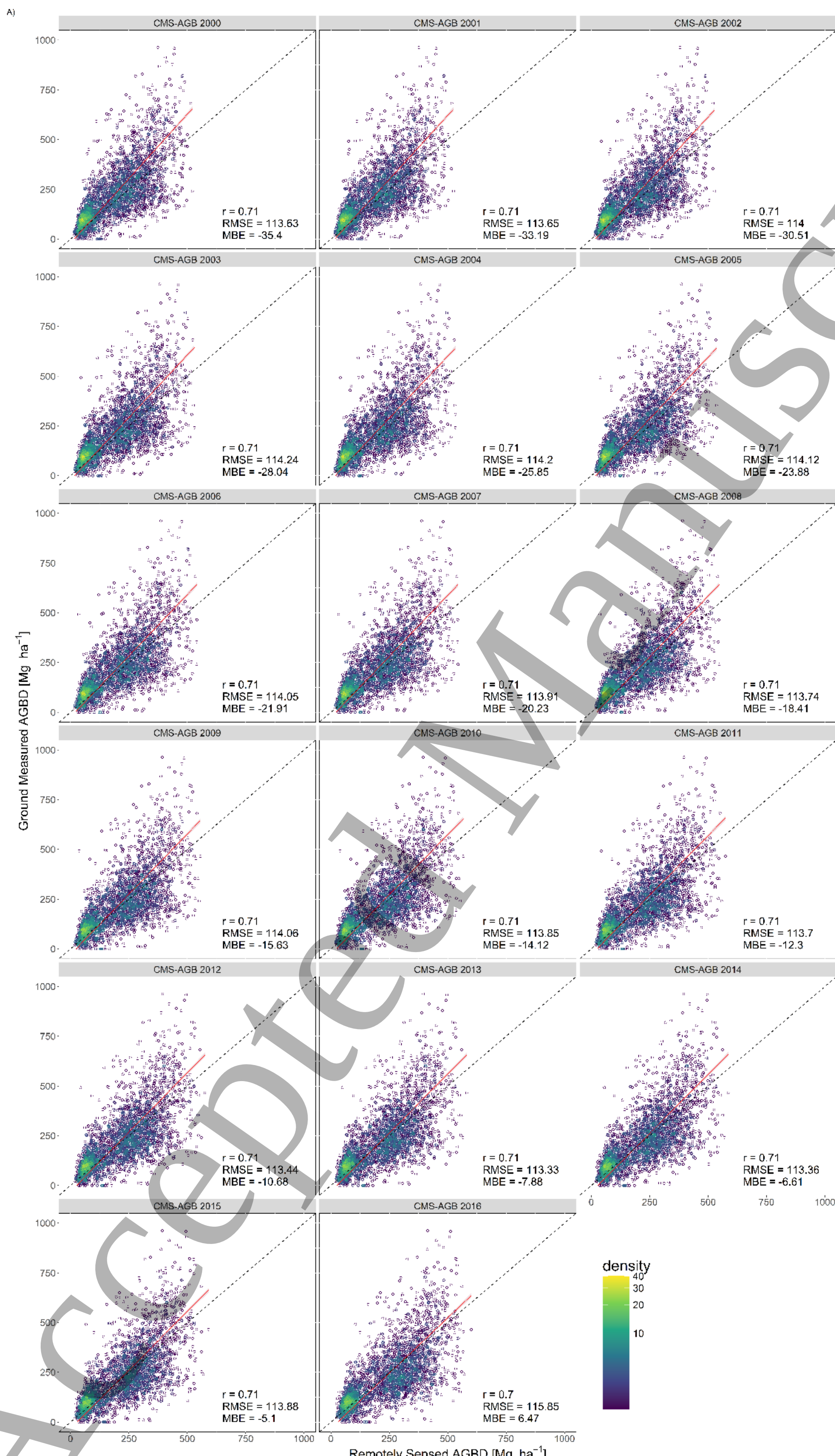
A)
CMS-AGB 2000
r = 0.71
RMSE = 113.63
MBE = -35.4
CMS-AGB 2001
r = 0.71
RMSE = 113.65
MBE = -33.19
CMS-AGB 2002
r = 0.71
RMSE = 114
MBE = -30.51
CMS-AGB 2003
r = 0.71
RMSE = 114.24
MBE = -28.04
CMS-AGB 2004
r = 0.71
RMSE = 114.2
MBE = -25.85
CMS-AGB 2005
r = 0.71
RMSE = 114.12
MBE = -23.88
CMS-AGB 2006
r = 0.71
RMSE = 114.05
MBE = -21.91
CMS-AGB 2007
r = 0.71
RMSE = 113.91
MBE = -20.23
CMS-AGB 2008
r = 0.71
RMSE = 113.74
MBE = -18.41
CMS-AGB 2009
r = 0.71
RMSE = 114.06
MBE = -15.63
CMS-AGB 2010
r = 0.71
RMSE = 113.85
MBE = -14.12
CMS-AGB 2011
r = 0.71
RMSE = 113.7
MBE = -12.3
CMS-AGB 2012
r = 0.71
RMSE = 113.44
MBE = -10.68
CMS-AGB 2013
r = 0.71
RMSE = 113.33
MBE = -7.88
CMS-AGB 2014
r = 0.71
RMSE = 113.36
MBE = -6.61
CMS-AGB 2015
r = 0.71
RMSE = 113.88
MBE = -5.1
CMS-AGB 2016
r = 0.7
RMSE = 115.85
MBE = 6.47
Ground Measured AGBD [Mg ha$^{-1}$]
Remotely Sensed AGBD [Mg ha$^{-1}$]
0
250
500
750
1000
density
40
30
20
10

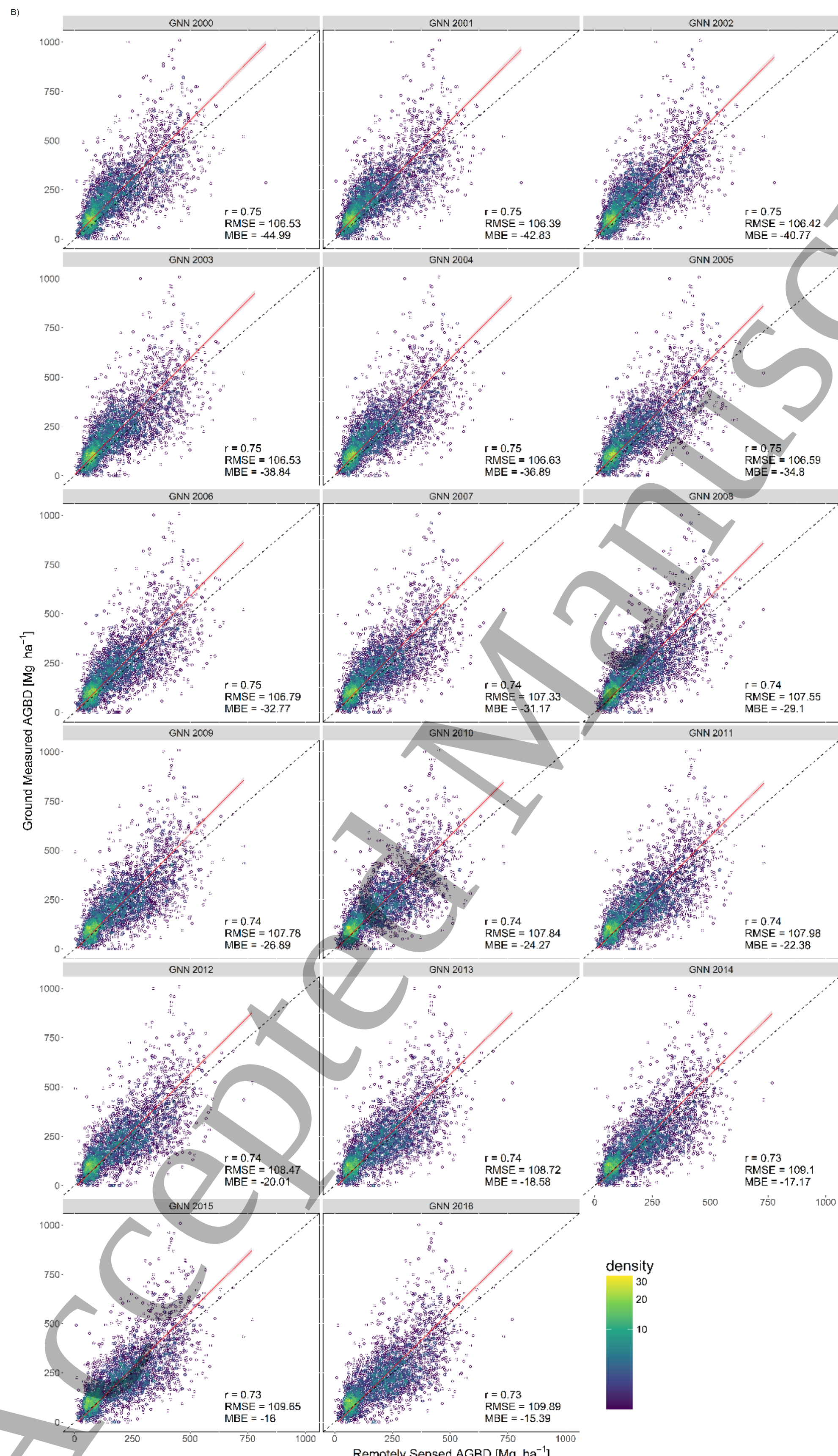
B)
GNN 2000
r = 0.75
RMSE = 106.53
MBE = -44.99
GNN 2001
r = 0.75
RMSE = 106.39
MBE = -42.83
GNN 2002
r = 0.75
RMSE = 106.42
MBE = -40.77
GNN 2003
r = 0.75
RMSE = 106.53
MBE = -38.84
GNN 2004
r = 0.75
RMSE = 106.63
MBE = -36.89
GNN 2005
r = 0.75
RMSE = 106.59
MBE = -34.8
GNN 2006
r = 0.75
RMSE = 106.79
MBE = -32.77
GNN 2007
r = 0.74
RMSE = 107.33
MBE = -31.17
GNN 2008
r = 0.74
RMSE = 107.55
MBE = -29.1
GNN 2009
r = 0.74
RMSE = 107.78
MBE = -26.89
GNN 2010
r = 0.74
RMSE = 107.84
MBE = -24.27
GNN 2011
r = 0.74
RMSE = 107.98
MBE = -22.38
GNN 2012
r = 0.74
RMSE = 108.47
MBE = -20.01
GNN 2013
r = 0.74
RMSE = 108.72
MBE = -18.58
GNN 2014
r = 0.73
RMSE = 109.1
MBE = -17.17
GNN 2015
r = 0.73
RMSE = 109.65
MBE = -16
GNN 2016
r = 0.73
RMSE = 109.89
MBE = -15.39
Ground Measured AGBD [Mg ha$^{-1}$]
Remotely Sensed AGBD [Mg ha$^{-1}$]
density
30
20
10

**Figure 3.** Ground-based AGBD observations regressed on mean AGBD estimates from A) CMS-AGB and B) GNN maps after aggregation at the stand level. The pink shaded area around the red solid line of best fit represents the 95% confidence interval. AGBD: Aboveground Biomass Density.

### 3.3. TreeMap and BIGMAP

Evaluation scale was an important factor for the comparison of the national TreeMap and BIGMAP products. TreeMap predictions were better correlated with observations (higher r) and were clearly more accurate (lower RMSE) and had less bias (lower MBE) than BIGMAP at the county level, but these differences were less at the hexagon level (table 2). At the local stand level, BIGMAP produced slightly higher r and lower RMSE, although TreeMap maintained a clearly lower MBE (figure 4). However, at the 3 point evaluation levels, BIGMAP produced the better fit statistics (table 2B). BIGMAP MBE notably varied, from being more negative than TreeMap at the county and hexagon levels, higher and positive at the stand level, and lower and positive at the 3 point evaluation levels. Meanwhile, TreeMap MBE remained lower than BIGMAP and consistently negative (table 2).

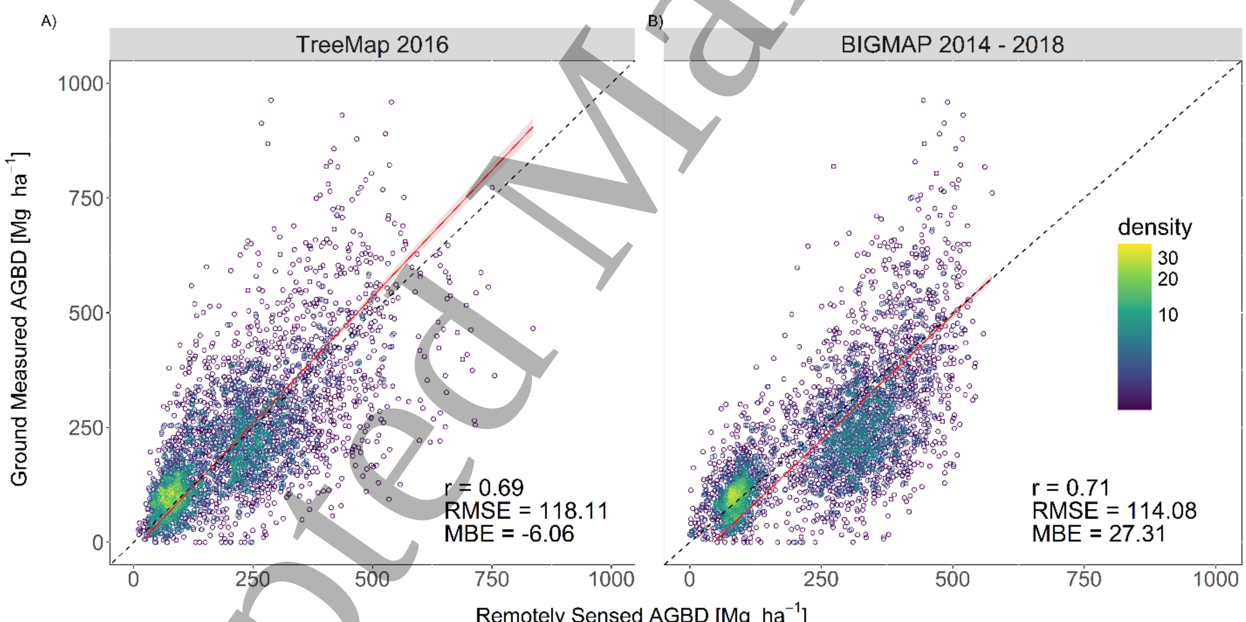


**Figure 4.** Ground-based AGBD observations regressed on mean AGBD estimates from A) TreeMap and B) BIGMAP maps after aggregation at the stand level. The pink shaded area around the red solid line of best fit represents the 95% confidence interval. AGBD: Aboveground Biomass Density.

### 3.4. MAXENT and ESACCI

The national MAXENT estimates trained from FIA data were less underpredicted than the global ESACCI estimates produced without using FIA data, in general across all evaluation levels (table 2). The important exception was that MAXENT overpredicted (positive MBE) AGBD at the stand level in all years except 2017, when MBE was slightly negative (figure 5, table S1). . Fit statistics varied little among the 5 MAXENT and 5 ESACCI maps with the exception of the 2010 ESACCI map, which performed better than the 2017-2020 ESACCI maps (figure 5, table S1).

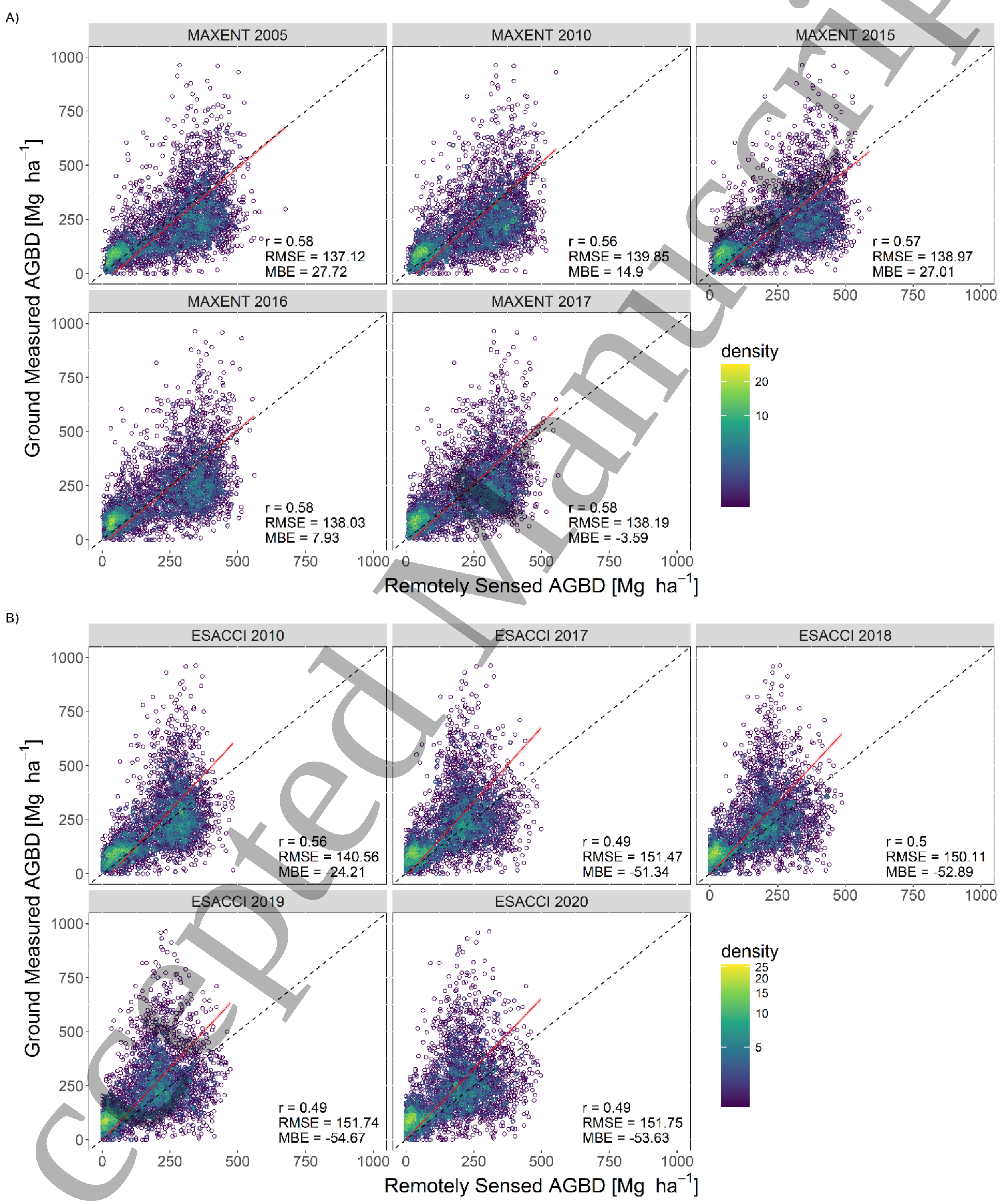


**Figure 5.** Ground-based AGBD observations regressed on mean AGBD estimates from A)

MAXENT and B) ESACCI maps after aggregation at the stand level. The pink shaded area around the red solid line of best fit represents the 95% confidence interval. AGBD: Aboveground Biomass Density.

### 3.5. ED and GEDI

GEDI-based maps consistently outperformed ED-based maps across most scales, especially the local stand (figure 6) and point levels (table S1), with lower RMSE and MBE and higher r. At the county level, MBE was negative (underprediction) from the GEDI and GEDI-informed ED maps, but the ED maps switched to positive (overprediction) at the hexagon level (table S1). The ED maps showed an overall tendency to overpredict AGBD, which peaked at the stand level (figure 6), yet remained consistently high at the point evaluation levels, where ED estimates informed by ICESat2 exhibited higher bias (MBE) but also higher precision (lower RMSE) than ED estimates informed by GEDI (table S1).

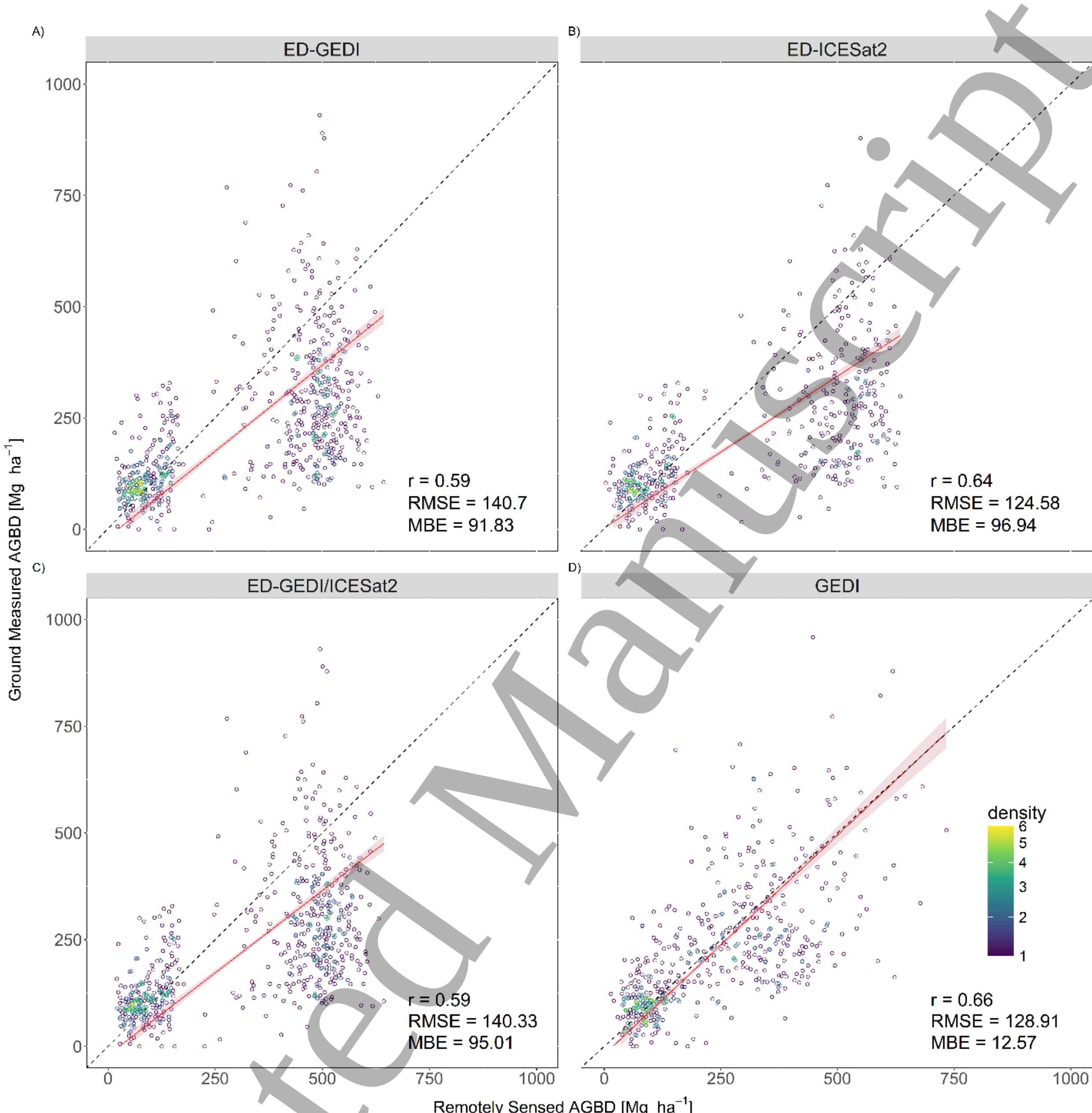


**Figure 6.** Ground-based AGBD observations regressed on mean AGBD estimates from A) ED-GEDI, B) ED-ICESat2, C) ED-GEDI/ICESat2, and D) GEDI maps after aggregation at the stand level. The pink shaded area around the red solid line of best fit represents the 95% confidence interval. There are noticeably fewer points because at the coarser resolution of these AGBD maps, fewer map pixel centers fall within the relatively small stand polygons. AGBD: Aboveground Biomass Density.

### 3.6. General Tree Aboveground Biomass Density (AGBD) Map Trends

Besides trends already described in the 5 paired comparisons, some general trends among the 10 AGBD maps are worth noting. At the county level, annual Landsat image-derived predictions

(GNN and CMS-AGB) produced the highest r and lowest RMSE statistics, followed closely by TreeMap, then the lidar-derived AGBD maps, then GEDI, BIGMAP, the MAXENT and ESACCI maps, and lastly ED. The 5 map types trained from FIA plot data (OR-LIDAR, GNN, TreeMap, BIGMAP, MAXENT) had higher r and lower RMSE statistics than the 5 map types that were not. MBE results were more erratic, with the lidar (OR-LIDAR, CMS-LIDAR), multispectral (CMS-AGB, GNN, TreeMap, BIGMAP), and ED maps generally performing best, followed by GEDI, and then the MAXENT and ESACCI products (table 2).

At the hexagon level, results exhibited more parity than at the other evaluation levels. The r and RMSE statistics are relatively consistent across all map types, with GNN performing the best and ESACCI the worst. In terms of MBE, the CMS-LIDAR and CMS-AGB maps performed well since they were explicitly calibrated to minimize bias, but TreeMap also performed well, whereas the coarser-scale products tuned to CONUS or larger extents exhibited the highest MBE, especially ESACCI and MAXENT (table 2).

All fit statistics except MBE notably worsened at local scales. At the stand level, and at the 3 point evaluation levels, the higher accuracy (low RMSE) of the lidar-derived AGBD maps (OR-LIDAR, CMS-LIDAR) clearly emerged, and r trended similarly. MBE trends were more variable and harder to interpret than RMSE trends at local levels. GEDI and BIGMAP were the AGBD products that had the smallest MBE, whereas ESACCI and ED had the largest MBE, albeit in the opposite directions of underprediction and overprediction, respectively (table 2).

**Table 2.** Summary statistics of agreement between ground-based observations regressed on mapped Aboveground Biomass Density (AGBD) predictions and evaluated at: A) 3 polygon levels and B) 3 point levels. More than one AGBD map was considered for 5 of the 10 AGBD map types, as indicated in the footnotes. Fit statistics for all individual maps are in table S1.

A)

| | County (N = 24) | | | | Hexagon (N = 179) | | | | Stand (N = 3496) | | | |
|---|---|---|---|---|---|---|---|---|---|---|---|---|
| | **AGB Map** | **r** | **RMSE (Mg/ha)** | **MBE (Mg/ha)** | **AGB Map** | **r** | **RMSE (Mg/ha)** | **MBE (Mg/ha)** | **AGB Map** | **r** | **RMSE (Mg/ha)** | **MBE (Mg/ha)** |
| | OR-LIDAR | 0.92 | 35.63 | 5.41 | OR-LIDAR | 0.84 | 61.57 | 13.81 | OR-LIDAR | 0.84 | 85.34 | 27.82 |
| | CMS-LIDAR | 0.86 | 46.8 | -17.23 | CMS-LIDAR | 0.83 | 63.05 | -2.21 | CMS-LIDAR | 0.83 | 86.86 | 30.74 |
| [1] | CMS-AGB | 0.95 | 27.99 | -12.43 | [1] CMS-AGB | 0.81 | 65.9 | -7.16 | [1] CMS-AGB | 0.71 | 113.94 | -17.84 |
| [1] | GNN | 0.95 | 26.98 | -19.06 | [1] GNN | 0.86 | 57.27 | -15.87 | [1] GNN | 0.74 | 107.66 | -28.99 |
| | TreeMap | 0.93 | 32.59 | -12.51 | TreeMap | 0.83 | 62.48 | -4.48 | TreeMap | 0.69 | 118.11 | -6.06 |
| | BIGMAP | 0.8 | 56.01 | -35.44 | BIGMAP | 0.82 | 65.17 | -15.45 | BIGMAP | 0.71 | 114.08 | 27.31 |
| [2] | MAXENT | 0.8 | 56.45 | -56.93 | [2] MAXENT | 0.78 | 71.49 | -39.95 | [2] MAXENT | 0.57 | 138.43 | 14.79 |
| [3] | ESACCI | 0.76 | 60.33 | -57.44 | [3] ESACCI | 0.73 | 78.86 | -53.29 | [3] ESACCI | 0.51 | 149.13 | -47.35 |
| [4] | ED | 0.74 | 63.62 | -6.57 | [4] ED | 0.79 | 68.88 | 23.54 | [4] ED | 0.61 | 135.2 | 94.59 |
| | GEDI | 0.83 | 51.08 | -33.45 | GEDI | 0.81 | 66.76 | -20.11 | GEDI | 0.66 | 128.91 | 12.57 |

B)

| | Plot (N = 2452) | | | | All Subplot (N = 9550) | | | | Center Subplot (N = 2404) | | | |
|---|---|---|---|---|---|---|---|---|---|---|---|---|
| | **AGB Map** | **r** | **RMSE (Mg/ha)** | **MBE (Mg/ha)** | **AGB Map** | **r** | **RMSE (Mg/ha)** | **MBE (Mg/ha)** | **AGB Map** | **r** | **RMSE (Mg/ha)** | **MBE (Mg/ha)** |
| | OR-LIDAR | 0.92 | 83.76 | 18.39 | OR-LIDAR | 0.81 | 148.49 | 17.93 | OR-LIDAR | 0.82 | 142.52 | 15.45 |
| | CMS-LIDAR | 0.9 | 93.05 | 21.48 | CMS-LIDAR | 0.79 | 154.77 | 21.28 | CMS-LIDAR | 0.79 | 154.66 | 19.62 |
| [1] | CMS-AGB | 0.69 | 159.66 | -24 | [1] CMS-AGB | 0.59 | 218.6 | -23.33 | [1] CMS-AGB | 0.59 | 219.23 | -27.14 |
| [1] | GNN | 0.86 | 109.13 | -26.72 | [1] GNN | 0.7 | 187.49 | -26.04 | [1] GNN | 0.71 | 183.67 | -30.32 |
| | TreeMap | 0.66 | 175.42 | -15.44 | TreeMap | 0.5 | 245.39 | -15.4 | TreeMap | 0.51 | 239.62 | -18.8 |
| | BIGMAP | 0.69 | 159.44 | 7.78 | BIGMAP | 0.6 | 215.65 | 8.03 | BIGMAP | 0.58 | 218.23 | 5.34 |

| | | | | | | | | | | | |
|---|---|---|---|---|---|---|---|---|---|---|---|
| [2] MAXENT | 0.56 | 190.61 | -25.98 | [2] MAXENT | 0.46 | 248.54 | -27.03 | [2] MAXENT | 0.44 | 253.19 | -29.77 |
| [3] ESACCI | 0.41 | 219.39 | -41.92 | [3] ESACCI | 0.33 | 276.82 | -42.94 | [3] ESACCI | 0.33 | 275.74 | -45.47 |
| [4] ED | 0.53 | 198.43 | 44.94 | [4] ED | 0.44 | 252.67 | 44.77 | [4] ED | 0.43 | 252.82 | 42.1 |
| GEDI | 0.61 | 178.52 | -1.89 | GEDI | 0.51 | 235.92 | -3.72 | GEDI | 0.51 | 236.52 | -7.08 |

[1] Means of 17 annual maps (2000-2016)

[1] Means of 17 annual maps (2000-2016)

[2] Means of 5 maps (2005, 2010, 2015, 2016, 2017)

[3] Means of 5 maps (2010, 2017, 2018, 2019, 2020)

[4] Means of 3 maps (GEDI, ICESAT2, GEDI & ICESAT2)

## 4. Discussion

This study evaluated 10 different AGBD map products in a smaller study area than is optimal for some of the maps, especially the globally tuned ED and ESACCI and near-global (tropical and temperate) GEDI maps. On the other hand, it is difficult to find airborne lidar-derived AGBD products systematically produced across large spatial extents, yet we considered it important to include airborne lidar-derived AGBD maps in this study, given lidar's reputation as the best available remote sensing technology for AGBD mapping. Our study area represents many of the diverse forest conditions found not only in the western US but across North America; therefore, we feel confident about generalizing inferences that can be drawn from our results.

Given the differences in how these 10 AGBD maps were modeled, and in the tree list data used to train some of the models (e.g., whether or not live saplings were included), it was much simpler to produce different validation datasets with or without live saplings than to reproduce already published AGBD maps with or without live saplings. However, the relative maturity and flexibility of the GNN modeling workflow made it easy to reproduce the annual GNN maps by applying the same tree training data constraints and F/NF mask as was used to produce the CMS-AGB maps (table 1).

### 4.1. OR-LiDAR and CMS-LiDAR

The CMS-LIDAR and CMS-AGB maps were trained from stakeholder-contributed inventory plot data. Due to concerns that the contributed plots do not constitute a representative sample and their use might introduce bias, the CMS-AGB map workflow used FIA data to calculate and apply a bias correction as the last step in map production (Hudak et al 2020). Thus, preliminary CMS-LIDAR and CMS-AGB maps were essentially calibrated to match FIA, such that the difference between the means (i.e., MBE) was minimized. The non-zero MBE in the CMS-LIDAR maps occurred because the spatial extent of our study area was smaller than the spatial extent across which the CMS-LIDAR maps were calibrated, which was the entire state of OR. In contrast, the OR-LIDAR map was trained using only those design-based FIA plots that intersected the combined spatial extent of the 20 lidar collections that also delimited our study area. Hence the OR-LIDAR map, which was more precisely aligned with the FIA plot training data, showed less bias than the CMS-LIDAR map across all evaluation levels (table 2), except hexagon (figure 2).

Our analysis up to this point has been more focused on the details of map production than on map utility, but the latter is an important consideration as well. Whether the AGBD map was trained from FIA data (OR-LIDAR) or not (CMS-LIDAR) could matter to a user depending on the application. Both of these maps could potentially be used to support local management decisions because they have been conditioned on FIA ground data, albeit by different strategies. However, some users may want to use the CMS-LIDAR AGBD map because it can be easily reverse engineered to restore its statistical independence from the FIA ground observations. The uncalibrated AGBD map is not publicly available, but by simply inverting and applying the published linear regression model equation used to calibrate the AGBD map (Fekety et al 2025), one can essentially uncalibrate the AGBD map. This makes it independent of FIA plot data and thus a good candidate for estimation methods that use FIA data and require independent covariates (Mauro et al 2022).

**4.2. CMS-AGB and GNN**

The CMS-AGB maps were calibrated in a manner similar to that of the CMS-LIDAR maps, but for the entire northwestern USA (OR, WA, ID and western MT), a region comparable in size and forest structural diversity to the GNN mapping extent, which included 3 West Coast states. In this comparison, we found the CMS-AGB maps to be slightly less biased (lower MBE) across all evaluation levels. However, the greater accuracy (lower RMSE) and closer fit (higher r) of the GNN maps is likely because they were trained using the same FIA data as were used at all evaluation levels–except stand-level, which offers the most objective comparison, because the ground observations are independent of FIA. Yet the same trend held as at the other evaluation levels, with the CMS-AGB maps showing less bias but also less accuracy than the GNN maps, which also maintained a closer fit to the ground observations (table 2).

The annual GNN maps performed very consistently across the 17-year range at all evaluation levels, as did the annual CMS-AGB maps, until the last map year (2016) (table S1). This can be attributed to not running LandTrendr through an additional year of the Landsat image time series to produce the CMS-AGB maps; i.e., through 2017, since the LandTrendr outputs are affected by the Landsat imagery not just in year *t* (e.g., 2016) but years *t*-1 and *t*+1 (e.g., 2017) (Fekety and Hudak 2019). It should also be noted that both the CMS-AGB and GNN maps exhibited slowly increasing AGBD predictions from 2000 to 2016 which, after subtracting the ground observations to calculate bias, causes the MBE statistic to become less negative (less underprediction) from 2000 to 2016 (table S1). This apparent AGBD drift, which is not seen in the concomitant ground observations, is mirrored most directly in a similar drift in visible band values of the source Landsat data and has been observed anecdotally in other regions (Robert Kennedy, *personal communication*). Its lack of relation to ground observations suggests a possible sensor artifact, but this can only be tested through a separate investigation of sensor calibration over time.

**4.3. TreeMap and BIGMAP**

TreeMap outperformed BIGMAP at the coarser county and hexagon scales encompassing multiple FIA plots, whereas BIGMAP performed better at the local scale of stands and individual FIA plots and subplots. Both products use FIA plot observations, but in different ways. BIGMAP uses spectral information to train a model to assign FIA plots to pixels based on multispectral similarity. TreeMap uses the FIA plots as the reference dataset in a RF model made with modeled LANDFIRE layers as predictors. While TreeMap imputations are based on a single most frequently occurring plot in the terminal nodes, BIGMAP imputations are based on multiple nearest neighbors and are produced through averaging. Furthermore, the BIGMAP predictors are the original remote sensing imagery whereas Treemap uses modeled predictors that contain propagated error (Riley 2022). These factors might explain the higher precision of BIGMAP at local evaluation levels. In addition, TreeMap uses categorical breaks in cover and height to partition the RF trees; this discretization of the predictor space can restrict the modeling process relative to the continuous nature of the BIGMAP continuous feature space approach.

Both products have features attractive to many users. TreeMap has been used to assess management tradeoffs between forest harvest targets and wildfire risk in the wildland urban-interface (Ager et al 2019), at the scale of the western US to model probability of bark beetle-caused tree mortality (Francis et al 2025), and nationally to map carbon emissions risk to communities (https://app.wildfireriskcarbon.org/home) and snag hazard risk to wildland fire responders (Riley et al 2022). BIGMAP products have been used for forest inventory (Bell et al 2022, Maxwell et al 2023, Westfall and Wilson 2022, Wilson 2025) and as well as several other applications including prescribed fire management (Gould et al 2023), wildlife habitat preference mapping (McGraw 2023), and hurricane risk mapping (Tumber-Dávila et al 2024). Both BIGMAP and TreeMap are fundamentally maps of imputed FIA plot IDs that can be related to tree lists, to facilitate map integration with forest growth models such as the Forest Vegetation Simulator (Dixon 2002) and more flexible analyses combining multiple variables.

### 4.4. MAXENT and ESACCI

The 5 iterations of MAXENT maps produced consistent fit statistics at all evaluation levels except the stand level, where 4 of the 5 maps flipped to overpredicting AGBD instead of underpredicting as in all other cases. This is surprising because only at the stand level are the MAXENT predictions independent of the FIA ground observations, yet this evaluation level exhibited the lowest MBE. The more negative MBE of the ESACCI maps were consistent among the 5 map iterations at all evaluation levels (table S1). The weak sensitivity of the SAR signal to high biomass forests could lead to the uncertainty of the MAXENT and ESACCI models that causes moderate to large estimation biases.

Regardless of lower accuracy, one point to consider with MAXENT and ESACCI products is the practicality of producing periodic AGBD estimates at the national scale of CONUS. MAXENT could be the better choice based on our evaluation for applications up to the national scale. But for applications over larger areas, or if statistical independence is required, the ESACCI products are an excellent choice. Unlike the MAXENT products trained from FIA data (the NFI data of the US), ESACCI products are produced independently of NFI data. Thus ESACCI (and other ancillary) data can be used in concert with NFI data in statistical or geostatistical approaches that require independent covariates. For example, Hunka et al (2025) demonstrated this in Mexico, where the ESACCI and GEDI map products served as covariates in a model used for predicting AGBD for the Mexican NFI. This methodology could be replicated in other countries having NFIs, thanks to the statistical independence of the ESACCI and GEDI maps from ground-based NFIs.

### 4.5. ED and GEDI

The OR study area turned out to poorly represent the accuracy of the ED maps across CONUS, as shown by Ma et al (2023); they also compared AGBD predictions to FIA ground observations at the hexagon level, but nationally, and found the highest overprediction biases were in western OR (much of our study area), whereas the lowest underprediction biases were in the Sierra Nevada and upper Great Lakes regions. Across CONUS, mean AGBD estimation bias was -10 Mg/ha (Ma et al 2023).

Across all evaluation levels and fit statistics, the 1 km resolution GEDI map performed better than the 100 m resolution AGBD maps (ESACCI, MAXENT), despite having coarser spatial resolution. This result confirms the superiority of lidar above other remote sensing data types for estimation of AGBD (Lefsky et al 2001), even if GEDI data consist only of arrays of samples and not continuous coverage. AGBD is tightly coupled to canopy height that lidar measures, unlike passive optical or microwave imagery, or active SAR. This does not mean that synoptic canopy height rasters derived from integrating satellite lidar samples with other types of remotely sensed imagery would not have tremendous value for AGBD mapping, particularly as covariates that could be ingested into most of the AGBD mapping methodologies considered in this study. Successful integration of GEDI with optical (Potapov et al 2021) and interferometric SAR (Qi et al 2025) imagery have already been demonstrated outside our OR study area.

### 4.6. Uncertainty

Across the map products assessed, rankings of the map products based on their performance metrics were similar at the 3 polygon scales (i.e., county, hexagon, and stand). This is not surprising at the county and hexagon evaluation levels, which used publicly available validation data aggregated from design-based FIA plot data. However, the FSVeg database of stand-level estimates was derived not from plots chosen with a random or systematic sampling design, but rather stands that are purposely chosen for inventory. Nevertheless, trends in FSVeg-based estimates in comparison to the AGBD maps were largely consistent with the FIA-based estimates at larger (county and hexagon) aggregation scales. This is good news for land managers operating at project scales at which FIA plot estimates are simply too sparse to be very helpful. Our results argue for broader use of FSVeg stand estimates for evaluating regional raster map products, and at local scales, where FSVeg stand evaluation metrics also trended similarly to FIA plot and subplot metrics but at locations not available to the public.

The benefits of aggregation are also evident when comparing RMSE statistics between the FIA plot, subplot, and center subplot evaluation levels, across all AGBD map types. RMSE especially is improved when based on the plot-level aggregation of 4 subplot-level AGBD observations, each associated with 4 adjacent 30 m mapped AGBD estimates. FIA's systematic subplot configuration assures that heterogeneous forest structure sampled on the ground and imaged in the scene is captured, despite the small size of an FIA subplot (168 $m^2$) relative to a 30 m pixel (900 $m^2$). For this reason, the FIA plot layout can thus characterize an area that encompasses multiple pixels while minimizing field effort, assuming the subplot locations are accurately determined. It is important to emphasize that we used the confidential (accurate) FIA plot locations for the 3 point-level evaluations, and also in the interest of accuracy, limited these to plots measured within +/- 3 years of remote sensing data acquisition.

It is to be expected that AGBD map products trained from FIA data should produce better fit statistics upon validation with plot-based estimates also summarized from FIA data. Conversely, the CMS-LIDAR and CMS-AGB maps trained from stakeholder-contributed plot data should exhibit worse fit statistics. This would partially explain the lower accuracy (RMSE) of CMS-LIDAR and CMS-AGB estimates compared to paired OR-LIDAR and GNN estimates, respectively. Ohmann and Gregory (2002) reported plot-level RMSE that was 10% higher for GNN than in this study, based on an accuracy assessment procedure that did not allow a plot to self-impute–as likely occurred in this analysis. Self-imputation can occur if a plot used to train a *k*NN model can itself be the nearest neighbor, which would improve the fit statistics for GNN maps (and other maps trained from FIA plot data). On the other hand, using FIA data to calibrate the CMS-LIDAR and CMS-AGB *maps late* in the production process through regional correction coefficients avoided self-imputation and resulted in slightly lower MBE, as opposed to calibrating the *models early* in the production process using FIA data (potential self imputation) for the OR-LIDAR and GNN estimates.

Half of the 10 map types we considered were trained using FIA plot data (table 1) following a systematic sampling design. This is hugely advantageous for ensuring global map accuracy, but accuracy is still not assured locally, because the scale of local AGBD variation is finer than the nominal 5.26 km spatial sampling interval of FIA plots. Our results show that AGBD maps trained with FIA data and predicted from lidar or multispectral imagery (OR-LIDAR, GNN) were not clearly more or less biased across evaluation levels than those not trained with FIA plot data (CMS-LIDAR, CMS-AGB). High uncertainty in the ground-based AGBD estimates, even at the relatively large aggregation scale of the hexagons (Figs. 2-6), translates into more variable MBE statistics than RMSE statistics, when comparing between the different AGBD map types (table 2). It is therefore harder to make inferences about the bias than the accuracy of the AGBD maps. We did use the USDA Forest Service's Landscape Change Monitoring System (LCMS) (Housman et al 2025) disturbance maps (2000-2022) to explore whether wildfires (and other disturbances) may have influenced our results. However, the largest wildfire years over this period were 2018 and especially 2021, when 1% and 4% of the study area (and systematic FIA plots) burned respectively, but these proportions are unlikely to impact conclusions drawn from this study. Furthermore, the years 2018 and 2021 could only have marginally influenced the BIGMAP, ESACCI, ED, and GEDI maps, since the temporal ranges of the input data informing all the other AGBD maps predate 2018 (table 1).

Allometric error can contribute a great deal to uncertainty at the population level (Menlove and Healey 2020), but we controlled for allometric variation in our study by consistently using tree-level AGBD estimates derived from the CRM method (Woodall et al 2011) at all evaluation levels except the stand level. FIA has since incorporate newer approaches with which to derive their allometric models, known as the National Scale Volume Biomass (NSVB) models (Westfall et al 2024), but the AGBD maps considered in this study were produced prior to the switch from CRM to NSVB models. An exception is that the near-global GEDI map uses biomass allometric equations based on tree bole diameters (Jenkins et al 2003) along with similar biomass equations from outside CONUS (Duncanson et al 2022). Kennedy et al (2018) found AGBD estimates calculated using Jenkins et al (2003) are 16% higher than AGBD estimates calculated using the CRM method. For the stand-level evaluation, we calculated AGBD with FFE-FVS that uses localized allometries, which for the geographic variants that intersect our OR study area, can produce AGBD estimates up to 9% higher than CRM (Woodall et al 2011). Thus, Jenkins would be the larger source of overestimation bias relative to CRM, as found by Menlove and Healey (2020) and corroborated by this study in OR (figure S1). Figure S1 illustrates the degree to which allometric uncertainty can be a major source of bias and indicates that this topic deserves the attention of both AGBD map developers and users (Duncanson et al 2017, Stovall et al 2018, Johnson et al 2025).

Finally, it is important to note that the AGBD values for our evaluation units (counties, hexagons, stands, plots and subplots) are not from exhaustive measurements; they are, in effect, based on a subsample of the area attributed to the analysis unit. In the case of counties, hexagons, and plots, the subsample is based on a spatially balanced sample of an area that corresponds with a pixel summary. In the case of stands, subplots are systematically located within the stand that would align with the pixels aggregated within the stand, assuming the stand delineation is accurate. The implications of this vary, and include an unequal weight, or sample intensity (hectares per plot or stand) of each unit. This can be due to random assignment of plots, random (or nonrandom) nonresponse, and factors such as stratification imposed on the sampling design but not relevant to the use of sample units for map validation. All of these factors should be considered when using ground sample data as we have in this study.

### 4.7. Broader Inferences

Carbon monitoring requires ground observations as much as remote sensing data. It is the ground data which permit calculation of robust uncertainty estimates associated with AGBD maps (Hunka et al 2024). Encouragingly, most new NFI implementations since 2005 have targeted critical ecosystems, such as those found in tropical forest countries (Nesha et al 2021, 2022). Tropical forests are less understood because many are in developing countries that are less able to implement and maintain NFIs given that ground plots are laborious, time-consuming, and expensive to collect. Fortunately, there exist many funding mechanisms that can support developing countries to more accurately, objectively, and transparently assess and monitor their forest resources (Herold et al 2019). Requirements of many forest monitoring funding schemes include estimation of AGBD uncertainty, and our research can help inform not only US but other partner countries' efforts to better characterize their forests through integration of ground and remote sensing data.

Some AGBD mapping methods (i.e., CMS-LIDAR, CMS-AGB, ESACCI) leverage AGBD estimates that are statistically independent from the NFI data, as is required for modeling approaches that integrate NFI and remote sensing data, such as model-assisted inference (Ståhl et al 2016, Emick et al 2023, Hou et al 2023), or model-based approaches that exploit spatial autocorrelation to explain further AGBD variation, such as Bayesian inference (Babcock et al 2021, Emick et al 2023, Hunka et al 2024). The ESACCI map is particularly noteworthy and valuable in this regard, in that not only is it a global product with a temporal component, but it relies minimally on ground-based AGBD estimates. Indeed, it only uses tabular AGBD means summarized from national-level country reports to define the Bayesian priors used to calibrate the approach (Santoro et al 2024). The coarser resolution ED and GEDI AGBD map products are also noteworthy for their statistical independence from NFI data, making them suitable for model-assisted or model-based inference in concert with NFI data. In addition, among the methods represented, the ED approach was unique in that it utilized a process-based ecosystem model designed for dynamic carbon monitoring and modeling, rather than a statistical approach, to quantify AGBD.

The purpose of our study was to provide forest managers with contextual information to assist them with choosing an AGBD map from among several existing alternatives. While a single AGBD map provides enough information for most managers, some may wish to consider several maps, making an ensemble strategy another valid approach. Healey et al (2018) demonstrated the utility of an ensemble approach for mapping land cover disturbances at the scale of CONUS; that work forms the theoretical basis behind the LCMS map product. LCMS is based on an ensemble strategy that bundles different disturbance mapping methods and their associated uncertainties into a product that is superior to any single method. LCMS methods and data distribution strategies could provide a template for how AGBD mapping systems might be implemented.

## 5. Conclusion

There are no true forest censuses to compare map products against, making the use of ground sample data for evaluation of AGBD map products a challenging endeavor. The forest definitions and extents of each dataset can differ, as can the ground calibration and remote sensing data, impeding direct comparisons. Because of these challenges, we summarized gridded AGBD map products and ground observations at several polygon and point evaluation levels.

Our assumption going into this study is that most forest AGBD map users who make and implement management decisions are doing so locally, particularly at the forest stand level, which by design represents a forest management decision space. Our chosen study area in OR is limited to temperate coniferous forest types, but offers a wealth of ground and remote sensing data and provides the opportunity to systematically compare and evaluate 10 fundamentally different AGBD map types. It also features robust ground-based AGBD datasets, from stand-level data collected on managed forest lands, to NFI data at both finer plot/subplot levels and coarser county/hexagon levels. Our main novel findings are that AGBD map utility depends more on map extent than resolution, and that the scale of evaluation matters at least as much (if not more) for influencing a management decision, as the modeling approach or remote sensing data type used to develop the AGBD map product. For instance, lidar-based maps may well be more accurate locally, but that does not translate into greater accuracy or utility over broader areas. Our methods provide a framework for comparing AGBD maps elsewhere and our results point to important factors that AGBD map users should consider when choosing a map to use in support of land management activities.

**Acknowledgments**

This study was a product of the Biomass Working Group of the NASA CMS Science Team. Funding support was provided by NASA's Carbon Monitoring System (CMS) Program (Awards NNH15AZ06I, 80HQTR20T0002, NNH24OB24A, NNH20ZDA001N, 80NSSC25K7221, and 80NSSC21K1059). Additional support was provided by the GEDI Competed Science Team (Award 8080NSSC24K0599), the Joint Fire Science Program (Awards 15-S-01-01 and 22-2-02-15) and the Gordon and Betty Moore Foundation (Award 11974). This paper also is a contribution of the Western Fire and Forest Resilience Collaborative. Accurate FIA plot locations for use in support of CMS project work were provided through Memorandums of Cooperation signed by Hudak with the Pacific Northwest Research Station's Resource Monitoring and Assessment Program and the Rocky Mountain Research Station's Inventory and Monitoring Program.

**Data availability statement**

All AGBD maps considered in this study are publicly available; see footnotes below table 1.

**ORCID iDs**

Jeff Atkins https://orcid.org/0000-0002-2295-3131
Chad Babcock https://orcid.org/0000-0001-9597-4462
Jennifer Bakken https://orcid.org/0000-0002-6712-3086
David Bell https://orcid.org/0000-0002-2673-5836
Benjamin Bright https://orcid.org/0000-0002-8363-0803
John Byrne https://orcid.org/0000-0002-2026-3225
Grant Domke https://orcid.org/0000-0003-0485-0355

Laura Duncanson https://orcid.org/0000-0003-4031-3493
Patrick Fekety https://orcid.org/0009-0003-3225-2464
Matthew Gregory https://orcid.org/0000-0002-2522-7872
Sean Healey https://orcid.org/0000-0003-3498-4266
Rachel Houtman https://orcid.org/0000-0003-2097-9423
Andrew Hudak https://orcid.org/0000-0001-7480-1458
Neha Hunka https://orcid.org/0009-0006-3963-0933
George Hurtt https://orcid.org/0000-0001-7278-202X
Robert Kennedy https://orcid.org/0000-0002-5507-474X
Andrew Lister https://orcid.org/0000-0002-0412-7039
Lei Ma https://orcid.org/0000-0002-3959-4155
Francisco Mauro https://orcid.org/0000-0002-7832-6268
Roy Mita https://orcid.org/0009-0002-4457-3073
Brett Raczka https://orcid.org/0000-0003-0582-1118
Karin Riley https://orcid.org/0000-0001-6593-5657
Sassan Saatchi https://orcid.org/0000-0001-8524-4917
Maurizio Santoro https://orcid.org/0000-0002-3339-6991
John Shaw https://orcid.org/0000-0002-5797-1006
Carlos Silva https://orcid.org/0000-0002-7844-3560
Hao Tang https://orcid.org/0000-0001-7935-5848
Brian Walters https://orcid.org/0000-0001-7408-9704
Barry Wilson https://orcid.org/0000-0002-1940-7682
Aaron Weiskittel https://orcid.org/0000-0003-2534-4478
Yifan Yu https://orcid.org/0000-0001-6948-0493

## References

Ager A A, Houtman R M, Day M A, Ringo C and Palaiologou P 2019 Tradeoffs between US national forest harvest targets and fuel management to reduce wildfire transmission to the wildland urban interface *For. Ecol. Manage.* 434 99-109 https://doi.org/10.1016/j.foreco.2018.12.003

Babcock C, Finley A O and Looker N 2021 A Bayesian model to estimate land surface phenology parameters with harmonized Landsat 8 and Sentinel-2 images *Remote Sens. Environ.* 261 112471 https://doi.org/10.1016/j.rse.2021.112471

Bechtold W A and Patterson P 2005 The enhanced Forest Inventory and Analysis Program - national sampling design and estimation procedures. USDA Forest Service General Technical Report GTR-SRS-80, Southern Research Station, Fort Collins, CO, 85 p.

Bell D M , Wilson B T, Werstak Jr. C E, Oswalt C M and Perry C H 2022 Examining k-nearest neighbor small area estimation across scales using national forest inventory data *Front. For. Glob. Change* 5 763422 https://doi.org/10.3389/ffgc.2022.763422

Buchhorn M, Smets B, Bertels L, Roo B D, Lesiv M, Tsendbazar N-E, Herold M and Fritz S 2020 Copernicus global land service: land cover 100m: collection 3: epoch 2019: globe [data set]

Zenodo https://doi.org/10.5281/zenodo.3939050
Bullock E L, Healey S P, Yang Z, Acosta R, Villalba H, Insfrán K P, Melo J B, Wilson S, Duncanson L, Næsset E and Armston J 2023 Estimating aboveground biomass density using hybrid statistical inference with GEDI lidar data and Paraguay's national forest inventory *Environ. Res. Lett.* 18(8) 085001 https://doi.org/10.1088/1748-9326/acdf03
Burrill E A, DiTommaso A M, Turner J A, Pugh S A, Christensen G, Kralicek K M, Perry C J, Lepine L C, Walker D M and Conkling B L 2024 The Forest Inventory and Analysis Database, FIADB user guides, volume: database description (version 9.4), nationwide forest inventory (NFI). U.S. Department of Agriculture, Forest Service. 1016 p. [Online]. Available at web address: https://research.fs.usda.gov/understory/forest-inventory-and-analysis-database-user-guide-nfi
Cohen W B, Maiersperger T K, Gower S T and Turner D P 2003 An improved strategy for regression of biophysical variables and Landsat ETM+ data *Remote Sens. Environ.* 84 561-571 10.1016/S0034-4257(02)00173-6
Davidson A and McKerrow A 2016 GAP/LANDFIRE National Terrestrial Ecosystems 2011: U.S. Geological Survey data release https://doi.org/10.5066/F7ZS2TM0
Dixon G E comp. 2002 (Revised: 23 September 2025) Essential FVS: A user's guide to the Forest Vegetation Simulator *Internal Rep.* Fort Collins, CO: U.S. Department of Agriculture, Forest Service, Forest Management Service Center 238 p https://www.fs.fed.us/fmsc/ftp/fvs/docs/gtr/EssentialFVS.pdf
Doraisami M, Domke G M and Martin A R 2024 Improving wood carbon fractions for multiscale forest carbon estimation. *Carbon Balance Manage.* 19 25 https://doi.org/10.1186/s13021-024-00272-2
Dubayah R O, Armston J Healey S P Yang Z Patterson P L Saarela S Stahl G Duncanson L and Kellner J R 2022 GEDI L4B Gridded Aboveground Biomass Density, Version 2. ORNL DAAC, Oak Ridge, Tennessee, USA https://doi.org/10.3334/ORNLDAAC/2017
Duncanson L, Huang W, Johnson K, Swatantran A, McRoberts R E and Dubayah R 2017 Implications of allometric model selection for county-level biomass mapping *Carbon Balance Manage.* 12 18 https://doi.org/10.1186/s13021-017-0086-9
Duncanson L, Kellner J R, Armston J, et al 2022 Development of global lidar aboveground biomass density models for NASA's Global Ecosystem Dynamics Investigation (GEDI) lidar mission *Remote Sens. Environ.* 270 112845. https://doi.org/10.1016/j.rse.2021.112845
Emick E, Babcock C, White G W, Hudak A T, Domke G M and Finley A O 2023 An approach to estimating forest biomass while quantifying estimate uncertainty and correcting bias in machine learning maps *Remote Sens. Environ.* 295 113678 https://doi.org/10.1016/j.rse.2023.113678
Fekety P A and Hudak A T 2019 Annual aboveground biomass maps for forests in the northwestern USA, 2000-2016 ORNL DAAC, Oak Ridge, Tennessee, USA https://doi.org/10.3334/ORNLDAAC/1719
Fekety P A and Hudak A T 2025 LiDAR-derived forest aboveground biomass maps, northwestern USA, 2002-2016, v2 ORNL DAAC, Oak Ridge, Tennessee, USA https://doi.org/10.3334/ORNLDAAC/2443
Fortin M 2021 Comparison of uncertainty quantification techniques for national greenhouse gas inventories *Mitig. Adapt. Strateg. Glob. Chang.* 26 7http://dx.doi.org/10.1007/s11027-021-

09947-4
Francis E J, Jung C G, Hicke J A, Hurteau M D 2025 Modeling the probability of bark beetle-caused tree mortality as a function of watershed-scale host species presence and basal area *For. Ecol. Manage.* 580 122549 https://doi.org/10.1016/j.foreco.2025.122549
Gould N P, Pomara L Y, Nepal S, Goodrick S L and Lee D C 2023 Mapping firescapes for wild and prescribed fire management: A landscape classification approach *Land* 12 2180 https://doi.org/10.3390/land12122180
Healey S P, Cohen W B, Yang Z, Brewer C K, Brooks E B, Gorelick N, Hernandez A J, Huang C, Hughes M J, Kennedy R E, Loveland T R, Moisen G G, Schroeder T A, Stehman S V, Vogelmann J E, Woodcock C E, Yang L and Zhu Z 2018 Mapping forest change using stacked generalization: an ensemble approach *Remote Sens. Environ.* 204 717-728 https://doi.org/10.1016/j.rse.2017.09.029
Healey S P, Patterson P L, Armston J 2023 Algorithm Theoretical Basis Document (ATBD) for GEDI Level-4B (L4B) Gridded Aboveground Biomass Density Version 2.1 (ORNL Distributed Active Archive Center) https://daac.ornl.gov/daacdata/gedi/GEDI_L4B_Gridded_Biomass_V2_1/comp/GEDI_L4B_ATBD_V2.0.pdf
Herold M and Skutsch M 2011 Monitoring, reporting and verification for national REDD+ programmes: two proposals *Environ. Res. Lett.* 6 014002 https://doi.org/10.1088/1748-9326/6/1/014002
Hicke J A, Jenkins J C, Ojima D S, Ducey M 2007 Spatial patterns of forest characteristics in the western United States derived from inventories. *Ecol. Appl.* 17 2387-2402 https://doi.org/10.1890/06-1951.1
Homer C *et al* 2020 Conterminous United States land cover change patterns 2001–2016 from the 2016 National land cover database *ISPRS J. Photogramm. Remote Sens.* 162 184–99 https://doi.org/10.1016/j.isprsjprs.2020.02.019
Hou Z, Yuan K, Ståhl G, McRoberts R E, Kangas A, Tang H, Jiang J, Meng J, Xu Q and Li Z 2023 Conjugating remotely sensed data assimilation and model-assisted estimation for efficient multivariate forest inventory *Remote Sens. Environ.* 299 113854 https://doi.org/10.1016/j.rse.2023.113854
Housman I W, Heyer J P, Hardwick E A, Leatherman L, Borja M O, Megown K, Ross J and Ruether B 2025 Forest Service Landscape Change Monitoring System Methods Version 2024.10 Gen. Tech. Rep. GO-10301-RPT1 Salt Lake City, UT: US Department of Agriculture, Forest Service, Geospatial Office 44 p https://data.fs.usda.gov/geodata/rastergateway/LCMS/LCMS_v2024-10_Methods.pdf
Huang W, Dolan K A, Swatantran A, Johnson K D, Tang H, ONeil-Dunne J, Dubayah R, and Hurtt G 2019 High-resolution mapping of aboveground biomass for forest carbon monitoring system in the Tri-State region of Maryland, Pennsylvania and Delaware, USA *Environ. Res. Lett.* 14 095002. https://doi.org/10.1088/1748-9326/ab2917
Hudak A T, Evans J S and Smith A M S 2009 Review: LiDAR utility for natural resource managers *Remote Sens.* 1934-951 https://doi.org/10.3390/rs1040934
Hudak A T, Fekety P A, Kane V R, Kennedy R E, Filippelli S K, Falkowski M J, Tinkham W T, Smith A M S, Crookston N L, Domke G, Corrao M V, Bright B C, Churchill D J, Gould P J, Kane J T, McGaughey R J and Dong J 2020 A carbon monitoring system for mapping regional, annual

aboveground biomass across the northwestern USA *Environ. Res. Lett.* 15 095003 https://doi.org/10.1088/1748-9326/ab93f9

Hunka N, May P, Babcock C, Rosa J A A, Soriano-Luna M Á, Saucedo R M, Armston J, Santoro M, Suarez D R, Herold M, Málaga N, Healey S P, Kennedy R E, Hudak A T, Duncanson L 2025 A geostatistical approach to enhancing national forest biomass assessments with Earth Observation to aid climate policy needs *Remote Sens. Environ.* 318 114557 https://doi.org/10.1016/j.rse.2024.114557

Huo X, Fox A M, Dashti H, Devine C, Gallery W, Smith W K, Raczka B, Anderson J L, Rogers A and Moore D J P 2024 Integrating state data assimilation and innovative model parameterization reduces simulated carbon uptake in the Arctic and Boreal region. *J. Geophy. Res.: Biogeosciences* 129 e2024JG008004. https://doi.org/10.1029/2024JG008004

Hurtt G C *et al* 2022 The NASA Carbon Monitoring System Phase synthesis: scope, findings, gaps and recommended next steps *Environ. Res. Lett.* 17 063010. https://doi.org/10.1088/1748-9326/ac7407

Hurtt G C, Ma L, Lamb R, Campbell E, Dubayah R O, Hansen M, Huang C *et al* 2024 Beyond MRV: combining remote sensing and ecosystem modeling for geospatial monitoring and attribution of forest carbon fluxes over Maryland, USA *Environ. Res. Lett.* 19 124058 https://doi.org/10.1088/1748-9326/ad9035

IPCC 2019 2019 Refinement to the 2006 IPCC Guidelines for National Greenhouse Gas Inventories Intergovernmental Panel on Climate Change, Hayama, Kanagawa, Japan Available online at: https://www.ipcc-nggip.iges.or.jp/public/2019rf/index.html

Jenkins J C, Chojnacky D C, Heath L S and Birdsey R A 2003 National-scale biomass estimators for United States tree species *For. Sci.* 49 12–35 https://doi.org/10.1093/forestscience/49.1.12

Johnson L K, Domke G M, Stehman S V, Mahoney M J and Beier C M 2025 From pixels to parcels: Flexible, practical small-area uncertainty estimation for spatial averages obtained from aboveground biomass maps *Remote Sens Environ.* 330 114951 https://doi.org/10.1016/j.rse.2025.114951

Kellner J R, Armston J and Duncanson L 2023 Algorithm Theoretical Basis Document for GEDI Footprint Aboveground Biomass Density *Earth Space Sci.* 10 e2022EA002516 https://doi.org/10.1029/2022EA002516

Kennedy R E, Ohmann J, Gregory M, Roberts H, Yang Z, Bell D M, Kane V, Hughes M J, Cohen W B, Powell S and Neeti N 2018 An empirical, integrated forest biomass monitoring system. *Environ. Res. Lett.* 13 025004. https://doi.org/10.1088/1748-9326/aa9d9e

Kennedy R E, Serbin S P, Dietze M C, Andersen H-E, Babcock C, Baker D F, Brown M E, Davis K J, Duncanson L, Feng S, Hudak A T, Liu J, Patterson P L, Raczka B, Cochrane M A, Sepúlveda Carlo E A, and Vargas R 2024 Characterizing and communicating uncertainty: lessons from NASA's Carbon Monitoring System *Environ. Res. Lett.* 19 123003. https://doi.org/10.1088/1748-9326/ad8be0

Kennedy R E, Yang Z and Cohen, W B 2010 Detecting trends in forest disturbance and recovery using yearly landsat time series: 1. LandTrendr—Temporal Segmentation Algorithms *Remote Sens. Environ.* 114 2897–2910 https://dx.doi.org/10.1016/j.rse.2010.07.008

La Puma I P (Ed.) 2023 LANDFIRE technical documentation: Open-File Report https://doi.org/10.3133/ofr20231045

Lefsky M A, Cohen W B and Spies T A 2001 An evaluation of alternate remote sensing products for forest inventory, monitoring, and mapping of Douglas-fir forests in western Oregon *Canadian J. Forest Res.* 31 78–87 https://doi.org/10.1139/x00-142

Ma L, Hurtt G, Ott L, Sahajpal R, Fisk J, Lamb R, Tang H, Flanagan S, Chini L, Chatterjee A and Sullivan J 2022 Global evaluation of the ecosystem demography model (ED v3.0) *Geoscientific Model Develop.* 15(5):1971–1994 https://doi.org/10.5194/gmd-15-1971-2022

Ma L, Hurtt G, Tang H, Lamb R, Lister A, Chini L, Dubayah R, Armston J, Campbell E, Duncanson L, Healey S, O'Neil-Dunne J, Ott L, Poulter B and Shen Q 2023 Spatial heterogeneity of global forest aboveground carbon stocks and fluxes constrained by spaceborne lidar data and mechanistic modeling *Glob. Change Biol.* 29 3378–3394 https://doi.org/10.1111/gcb.16682

Ma L, Hurtt G C, Tang H, Lamb R, Lister A J, Chini L P, Dubayah R O, Armston J, Campbell E, Duncanson L, Healey S P, O'Neil-Dunne J, Ott L, Poulter B and Shen Q 2022 Global Forest Aboveground Carbon Stocks and Fluxes from GEDI and ICESat-2, 2018-2021 ORNL DAAC, Oak Ridge, Tennessee, USA https://doi.org/10.3334/ORNLDAAC/2180

Mauro F, Hudak A T, Fekety P A, Frank B, Temesgen H, Bell D M, Gregory M J and McCarley T R 2021a Lidar derived above ground biomass (AGB) for 20 lidar acquisitions in Oregon. WIFIRE Commons https://wifire-data.sdsc.edu/dataset/above-ground-biomass-agb

Mauro F, Hudak A T, Frank B, Temesgen H, Bell D M, Gregory M J, McCarley T R and Fekety P A 2021b Regional modeling of forest fuels and structural attributes using airborne laser scanning data in Oregon *Remote Sens.* 13 261 https://doi.org/10.3390/rs13020261

Maxwell A E, Wilson B T, Holgerson J J and Bester M S 2023 Comparing harmonic regression and GLAD Phenology metrics for estimation of forest community types and aboveground live biomass within forest inventory and analysis plots *Int. J. Appl. Earth Obs. Geoinf.* 122 103435 https://doi.org/10.1016/j.jag.2023.103435

May P B, Dubayah R O, Bruening J M and Gaines G C 2024 Connecting spaceborne lidar with NFI networks: A method for improved estimation of forest structure and biomass *Int. J. Appl. Earth Obs. Geoinf.* 129 103797 https://doi.org/10.1016/j.jag.2024.103797

McGraw A 2023, October. Seeing the Forests through the Deer: A Regional Assessment of White-tailed Deer Browsing Preferences and the Impact on Forest Regeneration In *Northern Hardwood Conference* https://conferences.lib.unb.ca/index.php/nhc/article/view/667

Menlove J and Healey S P 2020. A comprehensive forest biomass dataset for the USA allows customized validation of remotely sensed biomass estimates *Remote Sens.* 12 4141 https://doi.org/10.3390/rs12244141

Menlove J and Healey S P 2021 CMS: Forest Aboveground Biomass from FIA Plots across the Conterminous USA, 2009-2019 ORNL DAAC, Oak Ridge, Tennessee, USA https://doi.org/10.3334/ORNLDAAC/1873

Nesha K, Herold M, Veronique De Sy, de Bruin S, Araza A, Málaga N, Gamarra J G P, Hergoualc'h K, Pekkarinen A, Ramirez C, Morales-Hidalgo D and Tavani R 2022 Exploring characteristics of national forest inventories for integration with global space-based forest biomass data *Sci. Tot. Environ.* 850 157788 http://dx.doi.org/10.1016/j.scitotenv.2022.157788

Nesha M K, Herold M, De Sy V, Duchelle A E, Martius C, Branthomme A, Garzuglia M, Jonsson O, and Pekkarinen A 2021 An assessment of data sources, data quality and changes in national forest monitoring capacities in the Global Forest Resources Assessment 2005-2020 *Environ. Res. Lett.* 16(5) 054029 https://doi.org/10.1088/1748-9326/ABD81B

Ohmann J L and Gregory M J 2002 Predictive mapping of forest composition and structure with direct gradient analysis and nearest neighbor imputation in coastal Oregon, USA *Can. J. For. Res.* 32 725–741 https://doi.org/10.1139/x02-011

Ohmann J L, Gregory M J, Roberts H M, Cohen W B, Kennedy R E and Yang Z. 2012. Mapping change of older forest with nearest-neighbor imputation and Landsat time-series. *For. Ecol. Manage.* 272 13–25. https://doi.org/10.1016/j.foreco.2011.09.021

Patterson P L, Healey S P, Ståhl G, Saarela S, Holm S, Andersen H E, Dubayah R O, Duncanson L, Hancock S, Armston J, Kellner J R, Cohen W B, and Yang Z 2019 Statistical properties of hybrid estimators proposed for GEDI - NASA's global ecosystem dynamics investigation *Environ. Res. Lett.* 14 065007 https://doi.org/10.1088/1748-9326/ab18df

Peterson D L and Waring R H 1994 Overview of the Oregon Transect Ecosystem Research Project *Ecol. Appl.* 4 211-225 https://doi.org/10.2307/1941928

Phillips S J, Anderson R and Sschapire R 2006 Maximum entropy modeling of species geographic distributions *Ecological Modelling* 190 231–59 https://doi.org/10.1016/j.ecolmodel.2005.03.026

Phillips S J and Dudík M 2008 Modeling of species distributions with Maxent: new extensions and a comprehensive evaluation *Ecography* 31 161–75 https://doi.org/10.1111/j.0906-7590.2008.5203.x

Picotte J J, Dockter D, Long J, Tolk B, Davidson A and Peterson B 2019 LANDFIRE remap prototype mapping effort: Developing a new framework for mapping vegetation classification, change, and structure *Fire* 2 35. https://doi.org/10.3390/fire2020035

Potapov P, Li X, Hernandez-Serna A, Tyukavina A, Hansen M C, Kommareddy A, Pickens A, Turubanova S, Tang H, Silva C E, Armston J, Dubayah R, Blair J B, Hofton M 2021 Mapping global forest canopy height through integration of GEDI and Landsat data *Remote Sens. Environ.* 253 112165 https://doi.org/10.1016/j.rse.2020.112165

Qi W, Armston J, Choi C, Stovall A, Saarela S, Pardina M, Fatoyinbo L, Papathanasiou K, Dubayah R 2025 Mapping large-scale pantropical forest canopy height by integrating GEDI lidar and TanDEM-X InSAR data *Remote Sens. Environ.* 318 114534 https://doi.org/10.1016/j.rse.2024.114534

Raczka B, Hoar T J, Duarte H F, Fox A M, Anderson J L, Bowling D R and Lin J C 2021 Improving CLM5.0 biomass and carbon exchange across the Western United States using a data assimilation system. *J. Adv. Modeling Earth Sys.* 13 e2020MS002421. https://doi.org/10.1029/2020MS002421

Rebain S A 2010 (revised October 23, 2025) The fire and fuels extension to the forest vegetation simulator: updated model documentation. *Internal Rep.* (Fort Collins, CO: U. S. Department of Agriculture, Forest Service, Forest Management Service Center) 413 p Riley K L, Grenfell I C and Finney M A 2016 Mapping forest vegetation for the western US using modified random forests imputation of FIA forest plots *Ecosphere* 7 e01472 https://doi.org/10.1002/ecs2.1472

Riley K L, Grenfell I C, Finney M A and Shaw J D 2021a TreeMap 2016: A tree-level model of the forests of the conterminous United States circa 2016 Fort Collins, CO: Forest Service Research Data Archive https://doi.org/10.2737/RDS-2021-0074

Riley K L, Grenfell I C, Finney M A and Wiener J M 2021b TreeMap, a tree-level model of conterminous US forests circa 2014 produced by imputation of FIA plot data *Sci. Data* 8 11

https://doi.org/10.1038/s41597-020-00782-x
Riley, K L, Grenfell I C, Shaw J D, and Finney M A. 2022 TreeMap 2016 dataset generates CONUS_wide maps of forest characteristics including live basal area, aboveground carbon, and number of trees per acre. *J. Forestry* 1-26 https://doi.org/10.1093/jofore/fvac022
Riley K L, O'Connor C D, Dunn C J, Haas J R, Stratton R D and Gannon B 2022 A national map of snag hazard to reduce risk to wildland fire responders *Forests* 13 1160 https://doi.org/10.3390/f13081160
Rollins M G 2009 LANDFIRE: a nationally consistent vegetation, wildland fire, and fuel assessment *Int. J. Wildland Fire* 18 235-249 https://doi.org/10.1071/WF08088
Santoro M and Cartus O 2023 ESA Biomass Climate Change Initiative (Biomass_cci): Global datasets of forest above-ground biomass for the years 2010, 2017, 2018, 2019 and 2020, v4 https://catalogue.ceda.ac.uk/uuid/af60720c1e404a9e9d2c145d2b2ead4e
Santoro M, Cartus O, Carvalhais N, Rozendaal D, Avitabilie V, Araza A, de Bruin S, Herold M, Quegan S, Rodríguez Veiga P, Balzter H, Carreiras J, Schepaschenko D, Korets M, Shimada M, Itoh T, Moreno Martínez Á, Cavlovic J, Cazzolla Gatti R, da Conceição Bispo P, Dewnath N, Labrière N, Liang J, Lindsell J, Mitchard E T A, Morel A, Pacheco Pascagaza A M, Ryan C M, Slik F, Vaglio Laurin G, Verbeeck H, Wijaya A and Willcock S 2021 The global forest above-ground biomass pool for 2010 estimated from high-resolution satellite observations *Earth Syst. Sci. Data* 13 3927-3950 https://doi.org/10.5194/essd-2020-148
Santoro M, Cartus O, Quegan S, Kay H, Lucas R M, Araza A, Herold M, Labrière N, Chave J, Rosenqvist Å, Tadono T, Kobayashi K, Kellndorfer J, Avitabile V, Brown H, Carreiras J, Campbell M J, Cavlovic J, Bispo P C, Gilani H and Seifert F M 2024 Design and performance of the climate change initiative biomass global retrieval algorithm *Sci. Remote Sens.* 10 100169 https://doi.org/10.1016/j.srs.2024.100169
Ståhl G, Saarela S, Schnell S, Holm S, Breidenbach J, Healey S P, Patterson P L, Magnussen S, Næsset E, McRoberts R E and Gregoire T G 2016 Use of models in large-area forest surveys: comparing model-assisted, model-based and hybrid estimation *Forest Ecosystems* 3 https://doi.org/10.1186/s40663-016-0064-9
Stovall A E, Anderson-Teixeira K J and Shugart H H 2018 Assessing terrestrial laser scanning for developing non-destructive biomass allometry *Forest Ecol. Manag.* 427:217–229 http://dx.doi.org/10.1016/j.foreco.2018.06.004
Tinkham W T, Mahoney P R, Hudak A T, Domke G M, Falkowski M J, Woodall C W and Smith A M S 2018 Applications of the United States Forest Inventory and Analysis dataset: a review and future directions *Can. J. Forest Res.* 48 1–18 https://doi.org/10.1139/cjfr-2018-0196
Tomppo E, Gschwantner T, Lawrence M and McRoberts R E 2010 National forest inventories: pathways for common reporting National Forest Inventories: Pathways for Common Reporting Springer, Netherlands https://doi.org/10.1007/978-90-481-3233-1
Tumber-Dávila S J, Lucey T, Boose E R, Laflower D, León-Sáenz A, Wilson B T, MacLean M G and Thompson J R 2024 Hurricanes pose a substantial risk to New England forest carbon stocks *Glob. Change Biol.* 30 17259 https://doi.org/10.1111/gcb.17259
Warton D I, Duursma R A, Falster D S and Taskinen S 2012 smatr 3 – an R package for estimation and inference about allometric lines *Methods Ecol. Evol.* 3 257-259 https://doi.org/10.1111/j.2041-210X.2011.00153.x
Warton D I, Wright I J, Falster D S and Westoby M 2006 Bivariate line-fitting methods for

allometry *Biological Reviews* 81 259-291 https://doi.org/10.1017/S1464793106007007

Westfall J A, Coulston J W, Gray A N, Shaw J D, Radtke P J, Walker D M, Weiskittel A R, MacFarlane D W, Affleck D L R, Zhao D, Temesgen H, Poudel K P, Frank J M, Prisley S P, Wang Y, Sánchez Meador, A J, Auty D and Domke G M 2024 A national-scale tree volume, biomass, and carbon modeling system for the United States Gen. Tech. Rep. WO-104 Washington, DC: US Department of Agriculture, Forest Service 37 p https://doi.org/10.2737/WO-GTR-104

Westfall J A and Wilson B T 2022 Nonresponse bias in change estimation: a national forest inventory example. *Forestry* 95 301-311 https://doi.org/10.1093/forestry/cpab056

White D, Kimerling A and Overton W 1992 Cartographic and geometric components of a global sampling design for environmental monitoring *Cart. Geog. Inf. Sys.* 19 5–22

Wilson B T 2025 Model-assisted estimation for national forest inventory via triangular tessellation *For. Ecol. Manage.* 123080 https://doi.org/10.1016/j.foreco.2025.123080

Wilson B T, Lister A J and Riemann R I 2012 A nearest-neighbor imputation approach to mapping tree species over large areas using forest inventory plots and moderate resolution raster data *For. Ecol. Manage.* 271 182-198 https://doi.org/10.1016/j.foreco.2012.02.002

Wilson B T, Woodall C W and Griffith D M 2013 Imputing forest carbon stock estimates from inventory plots to a nationally continuous coverage *Carbon Balance Manage*. 8 1 https://doi.org/10.1186/1750-0680-8-1

Wilson B T, Knight J F and McRoberts R E 2018 Harmonic regression of Landsat time series for modeling attributes from national forest inventory data *ISPRS J. Photogram. Remote Sens.* 137 29-46 https://doi.org/10.1016/j.isprsjprs.2018.01.006

Woodall C W, Heath L S, Domke G M, and Nichols M C 2011 Methods and equations for estimating aboveground volume, biomass, and carbon for trees in the U.S. forest inventory, 2010. Gen. Tech. Rep. NRS-88. Newtown Square, PA: U.S. Department of Agriculture, Forest Service, Northern Research Station. 30 p.

Yanai R D, Wayson C, Lee D, Espejo A B, Campbell J L, Green M B, Zukswert J M, Yoffe S B, Aukema J E, Lister A J, Kirchner J W and Gamarra J G P 2020 Improving uncertainty in forest carbon accounting for REDD+ mitigation efforts *Environ. Res. Lett.* 15 124002 https://doi.org/10.1088/1748-9326/abb96f

Yanai R D, Young A R, Campbell J L, Westfall J A, Barnett C J, Dillon G A, Green M B and Woodall C W 2023 Measurement uncertainty in a national forest inventory: results from the northern region of the USA *Can. J. For. Res.* 53 163–177 https://doi.org/10.1139/cjfr-2022-0062

Yu Y, Saatchi S, Domke G M, Walters B, Woodall C, Ganguly S, Li S, Kalia S, Park T, Nemani R, Hagen S C and Melendy L 2022 Making the US national forest inventory spatially contiguous and temporally consistent. *Environ. Res. Lett.* 17 065002 https://doi.org/10.1088/1748-9326/ac6b47

Yu Y, Saatchi S S, Walters B F, Ganguly S, Li S, Hagen S, Melendy L, Nemani R R, Domke G M and Woodall C W 2021 Carbon Pools across CONUS using the MaxEnt Model, 2005, 2010, 2015, 2016, and 2017 ORNL DAAC, Oak Ridge, Tennessee, USA https://doi.org/10.3334/ORNLDAAC/1752

Zolkos S G, Goetz S J and Dubayah R 2013 A meta-analysis of terrestrial aboveground biomass estimation using lidar remote sensing *Remote Sens. Environ.* 128 289-298 https://doi.org/10.1016/j.rse.2012.10.017